Satellite Monitoring of Natural Reforestation Efforts in China's Drylands

Graphical Abstract

Highlights

- We assess the success of natural reforestation in China's TNSP using satellite data

- We use microwaves and SIF to measure water and photosynthesis in dryland vegetation

- A strong correlation is found between reforestation and remote sensing data

- Natural reforestation is successful at increasing vegetation activity in arid areas
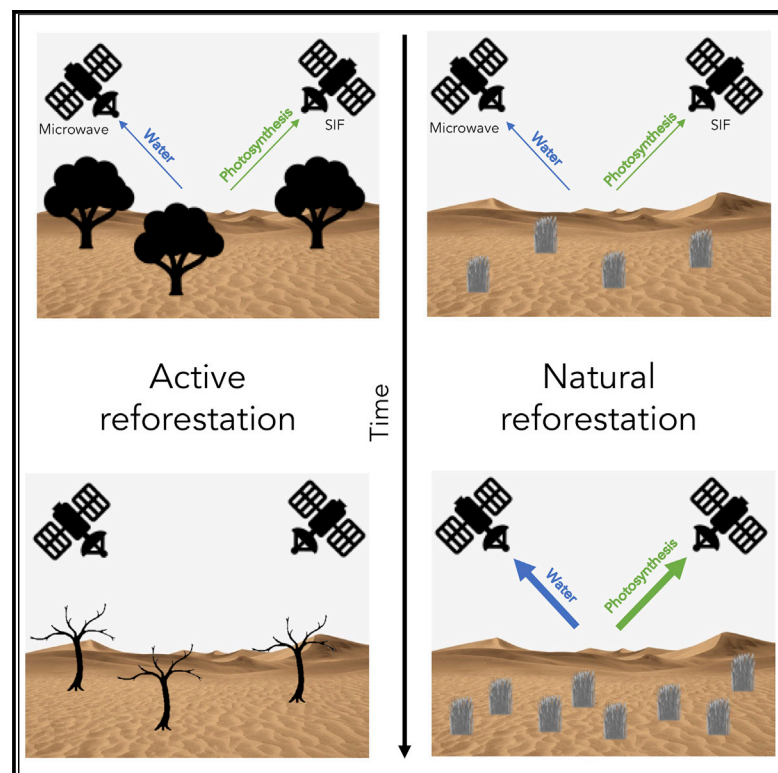
Authors

Cynthia Gerlein-Safdi,
Gretchen Keppel-Aleks, Feng Wang,
Steve Frolking, Denise L. Mauzerall

Correspondence

cgerlein@umich.edu

In Brief

China has been a leader in reforestation efforts with multiple large-scale projects. In this study, we found that satellite data sensitive to water and photosynthesis activity in plants in drylands is tightly linked to reforestation efforts in the Three-North Shelterbelt Program area. In particular, both traditional active reforestation and new natural reforestation increased vegetation activity. This is important because natural reforestation has advantages, such as increasing biodiversity. China's successful implementation of natural reforestation could become a model for other regions.

Satellite Monitoring of Natural Reforestation Efforts in China's Drylands

Cynthia Gerlein-Safdi,[1,2,7,*] Gretchen Keppel-Aleks,[1] Feng Wang,[3] Steve Frolking,[4,5] and Denise L. Mauzerall[2,6]

[1]Department of Climate and Space Sciences and Engineering, University of Michigan, Ann Arbor, MI 48109, USA
[2]Department of Civil and Environmental Engineering, Princeton University, Princeton, NJ 08544, USA
[3]Institute of Desertification Studies, Chinese Academy of Forestry, Beijing 100091, China
[4]Institute for the Study of Earth, Oceans, and Space, University of New Hampshire, Durham, NH 03824, USA
[5]Department of Earth Sciences, University of New Hampshire, Durham, NH 03824, USA
[6]Woodrow Wilson School of Public and International Affairs, Princeton University, Princeton, NJ 08544, USA
[7]Lead Contact
*Correspondence: cgerlein@umich.edu
https://doi.org/10.1016/j.oneear.2019.12.015

SCIENCE FOR SOCIETY Climate change has been driving desertification in many parts of the world, from the southwestern United States to Sub-Saharan Africa. Deserts often encroach over arable land, reducing income for farmers and causing dust storms with large health impacts on the local population and global climate effects. Reforestation efforts protect the sand from being lifted by the wind, but these projects often fail because these areas are very dry, and the plants do not survive. Understanding how well different strategies work in this harsh environment is of global interest because many countries use reforestation as an official offset for their CO_2 emissions. However, because of the mismatch between planted and surviving trees, the accounted carbon sequestered in these forests is overestimated. In this study, we use a new type of satellite data looking at vegetation water and photosynthesis to compare the success of different reforestation methods, using China's Three-North Shelterbelt Program as a case study.

SUMMARY

Desertification in Northern China degrades air quality in China's eastern cities by causing frequent dust storms. To stop desert expansion, China's government initiated the Three-North Shelterbelt Program, a large-scale reforestation project. Many issues with the project have been raised, from the choice of ill-adapted species to planting methods. Recently, the government implemented "natural reforestation"—closing former pastures to let vegetation regrow naturally. Unfortunately, it has been difficult to estimate the large-scale success of natural reforestation because measuring arid ecosystem productivity is a challenge for optical remote sensing. Here, we use satellite data to monitor vegetation water content and photosynthetic activity, thereby quantifying changes in vegetation biomass and productivity in Northern China. These satellite data corroborate official reforestation data. Our results show that vegetation activity is strongly correlated with both natural and traditional active reforestation, indicating opportunities for new natural reforestation techniques combined with satellite monitoring in other semi-arid regions.

INTRODUCTION

Desertification in arid or semi-arid areas has been an environmental issue in regions as geographically diverse as Northern China, the Sahel, or the southwestern United States.[1–3] Desertification is associated with anthropogenic causes,[4] such as overgrazing,[5–7] logging, or unsustainable agricultural practices,[2,8] and climate change,[9] specifically shifts in the spatial and temporal patterns of rainfall[10–12] and gale days (wind velocity greater than 17 m/s).[13,14] When combined, these effects can lead to rapid vegetation cover loss, and subsequent wind erosion can also cause large dust storms,[15] leading to increased fine particulate air pollution with associated adverse health impacts[16,17] and desert encroachment onto vegetated and inhabited areas.[18,19] In China, desertification has occurred mostly in the north of the country.[4,20–22] In response to the expanding desert, the Chinese government has implemented multiple large-scale projects. The Three-North Shelterbelt Program (TNSP, 1978 to 2050, Figure S1)[23–26] presents a unique challenge, because it is specifically focused on reforesting semi-arid ecosystems.

So far, very few studies have focused specifically on the TNSP, but the sparse evidence points at a mismatch between the very large increase in reforested area reported by the government[27,28] and the more modest increase observed from optical remote sensing.[29,30] A low survival rate of planted trees is usually assumed to explain this discrepancy.[28] However, dryland vegetation has a low greenness index (Figure S2) that makes it difficult for
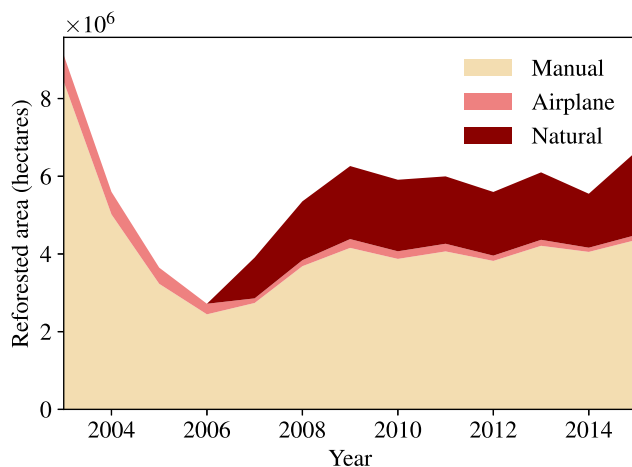
Figure 1. Evolution of the Total Reforested Area Classified by Reforestation Method

Reforestation data from the China Statistical Yearbooks[52] showing the area (hectares/year) reforested each year by manual planting, airplane planting, and natural reforestation for the entire TNSP area between 2003 and 2015.

optical remote sensing to capture, leading to an underestimation of vegetation cover.[31,32] Other concerns include the choice of planting method,[30] as well as the level of care given to the trees.[28]

In addition, the use of inappropriate species can deplete soil water,[33–35] potentially leading to widespread diebacks during droughts.[36,37] As a result, the scientific community in China and abroad has called for better planning from the government when designing projects.[38]

The most common form of reforestation in China is "active reforestation" through manual and airplane planting, either by local communities or occasionally by the military.[39] This technique has been especially successful in wetter areas in China where ecosystems are not water limited.[40–43] Recently, natural reforestation, i.e., closing of former pastures or fields to let the natural shrub savanna recover,[30,44,45] has become increasingly common. This new direction in China's reforestation effort is based on models and experiments showing that even dryland ecosystems should be able to recover if adverse human effects are removed.[46,47] However, because of its recent implementation, no data exist on how well natural reforestation does compared with active reforestation.

Assessing the success of natural reforestation without visiting the thousands of individual sites is indeed a challenge in itself, because of the inherent sparseness and low greenness index of the vegetation that make it difficult to map using traditional optical remote sensing (Figure S2) such as Landsat or vegetation indices from the Moderate Resolution Imaging Spectroradiometer (MODIS).[31,32] Here, we propose a novel use of active microwave remote sensing data from the QuikSCAT satellite[48] and solar-induced chlorophyll fluorescence (SIF)[49] from the Global Ozone Monitoring Experiment 2 (GOME-2) satellite[50,51] to examine vegetation water content and photosynthetic activity, respectively.

Here, we compare the trends in vegetation water and photosynthetic signals with the official reforestation statistics provided by the Chinese government.[52] We find that both vegetation

signals show an increase that is likely associated with an increase in vegetation cover over the years covered by the satellite data. In particular, we find strong correlations between vegetation indices and the increase in areas reforested through both active and natural reforestation techniques. Finally, a similar analysis is conducted using the Enhanced Vegetation Index (EVI) from MODIS,[53] and we find that both photosynthesis and water content are more strongly correlated with reforestation than EVI in the case of natural reforestation, but not for active reforestation, indicating that this new remote sensing product has the potential to improve our assessment of reforestation projects over drylands.

RESULTS

Reforestation Method Evolution

Over the past few decades, the Chinese government has continuously readjusted its planting strategies to increase survival rates. Planting data collected from the Yearbooks[52,54] is presented in Table S3 available in the Supplemental Information and summarized in Figure 1. We found that airplane planting was essentially abandoned by 2006, likely because of its low success rate. Manual planting experienced a sharp decline between 2003 and 2006, before stabilizing at around 4,000,000 hectares per year. Finally, natural reforestation was introduced in 2007 and quickly stabilized at around 2,000,000 hectares per year. In Inner Mongolia's sub-provinces,[54] similar trends were found, with very little use of airplane planting; a stable number of hectares was reforested by manual planting, and an increasing area was reforested through natural reforestation.

Temporal Evolution of Vegetation Water Content and Photosynthetic Activity

The amount of photosynthesis happening in leaves can be captured from satellites with SIF retrievals. As vegetation cover increases, so does the number of leaves and the strength of the SIF signal emitted. After correcting for signal drift (Figure S3 and Equation 2), SIF data show clear trends for the time period between the launch of the GOME-2 satellite in 2007 and 2017 (see Figure 2). Overall, the photosynthesis signal increased the most in the eastern side of the TNSP region, whereas the north and most of the west showed a small decline in SIF. These areas are the driest of the TNSP region, and this decline is likely caused by a decrease in vegetation cover due to the harsh environmental conditions.

Similar to photosynthesis, vegetation water content also increases with vegetation cover. The water content of leaves and branches can be captured by the backscattering cross-section of active microwave remote sensing (σ^0 usually expressed in dB). Over the TNSP area, the trends in QuikSCAT backscatter σ^0 between 2000 and 2009 showed a similar spatial pattern (Figure 3) as SIF, with the eastern region of the TNSP experiencing an increase in canopy water that is likely associated with an increase in vegetation cover. Over the same period, the western half of the TNSP area exhibited an overall decrease in σ^0. The observed pattern matches the mean annual precipitation distribution,[23] which shows that the western half of the TNSP receives less than 200 mm/year of rain, whereas the eastern half is wetter with some areas receiving up to 700 mm/year of rain.
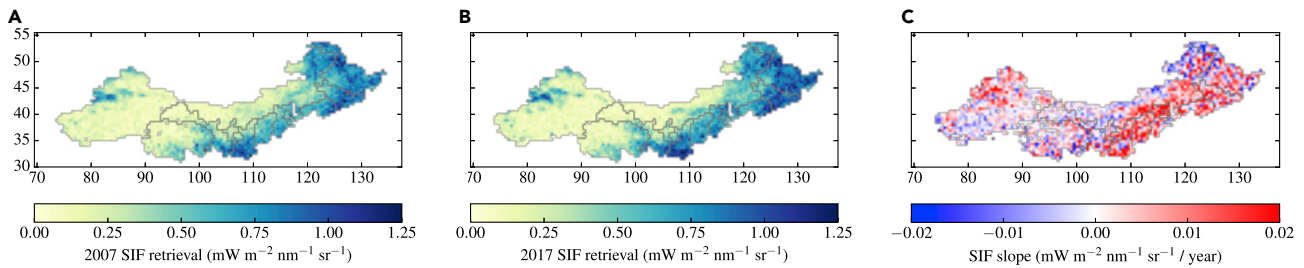
Figure 2. Maps of SIF Data for All 13 Provinces Involved in the TNSP
(A) Average SIF retrieval in 2007.
(B) Average SIF retrieval in 2017.
(C) Slope (mW/m²/nm/sr/year) of the best linear fit of the evolution of SIF retrievals between 2007 and 2017 (see Figure S4). An increase (decrease) in SIF corresponds to an increase (decrease) in photosynthesis that is likely due to an increase (decrease) in vegetation cover.

Comparison between σ^0 and SIF

While SIF and σ^0 reflect the photosynthesis activity and water content of the biomass, respectively, these quantities are tightly correlated in croplands.[55] Similarly, our analysis showed these quantities are generally correlated, albeit there are differences based on the MODIS land cover classification (Figures 4 and S9). Here, we combined different land cover types together: forest (n = 1,363) includes evergreen needleleaf, evergreen broadleaf, deciduous needleleaf, deciduous broadleaf, and mixed/other trees; low vegetation (n = 2,556) refers to closed shrublands, open shrublands, woody savannas, savannas, and grasslands; croplands (n = 1,006) includes both croplands and cropland/natural vegetation mosaics; and barren (n = 1,127) only includes pixels categorized as barren in the MODIS land cover map. Pixels categorized as urban and built-up land were removed from the QuikSCAT dataset, confirming that the method to exclude urban pixels using the σ^0 threshold worked as intended (see description in the section on Microwave Remote Sensing).

We found that there was a significant correlation between SIF and σ^0_{DH} (D, descending overpass; H, HH polarization) for all vegetated land use types ($R^2 = 0.16$, $p < 0.001$ in 2007, $R^2 = 0.11$, $p < 0.001$ in 2008, $R^2 = 0.20$, $p < 0.001$ in 2009), whereas no correlation was found for the barren land ($p = 0.16$ in 2007, $p = 0.39$ in 2008, $R^2 = 0.02$, $p < 0.001$ in 2009). Similar results were found with σ^0_{AV}, σ^0_{AH}, and σ^0_{DV} (A, ascending overpass; V, VV polarization). These results were anticipated, because barren lands are expected to have virtually no signal in SIF due to the lack of vegetation; but in non-vegetated areas, active microwave remote sensing is sensitive to variations in soil moisture and surface roughness.[56,57]

Correlation with Reforestation

Comparing the evolution of SIF data with reforestation data obtained from the Yearbooks, we found a strong correlation between the two (Figure 5). In particular, there was a similar correlation between photosynthetic activity from SIF and areas reforested by land closure, e.g., natural reforestation ($R^2 = 0.54$, $p < 0.0001$), then exists between SIF and active reforestation ($R^2 = 0.57$, $p < 0.0001$). σ^0_{DH} shows a much stronger correlation with natural reforestation than with active reforestation ($R^2 = 0.68$, $p < 0.0001$ for natural reforestation and $R^2 = 0.46$,

$p < 0.001$ for active reforestation), and similar results were obtained for the other data from QuikSCAT (Figure S7). In this case, Beijing City was removed from the analysis because it was a clear outlier, with an average σ^0_{DH} about three times as high as the other provinces. This is likely due to the limited extent of non-urban land and the strong impact of urban development on QuikSCAT data.[58] These results indicate that natural reforestation had a strong, positive impact on vegetation cover in the TNSP area that is comparable with the increase in vegetation cover from active reforestation.

Inner Mongolia Case Study

In the case of Inner Mongolia, we compared the sub-province-level evolution in SIF and σ^0_{DH} with the reforestation data obtained from the Inner Mongolia Yearbooks.[54] We found a strong, significant correlation between photosynthetic activity and reforestation efforts (Figure 6), both through natural reforestation ($R^2 = 0.52$, $p < 0.0001$) and active reforestation ($R^2 = 0.76$, $p < 0.0001$). Wuhai City was removed from the analysis in this case, because the footprint of the sub-province was smaller than a single SIF pixel. A similar analysis performed for σ^0_{DH} found a much weaker relationship with both natural reforestation ($R^2 = 0.14$, $p = 0.05$) and active reforestation ($R^2 = 0.16$, $p = 0.04$). Here, four outliers stand out: Wuhai City and Ordos City showed an increase in σ^0_{DH} greater than what would be expected based on the reforested area in each sub-province. One hypothesis is that the effect of urban expansion has not been fully removed from σ^0_{DH}[58] and is affecting the analysis at the sub-province level because of the small area considered compared with the province-level analysis. Hohhot and Ulaan Chab have very low σ^0_{DH} signals. Interestingly, these two sub-provinces showed the strongest correlation between yearly rainfall and average σ^0_{DH} (Figure S15). This would therefore indicate that at a finer spatial scale, the effects of rainfall and urban expansion can become a large source of signal in the QuikSCAT data, while the SIF data are not sensitive to these issues.

Effects of Rainfall

Besides an increase in forest cover due to reforestation, the observed increase in vegetation signal might also be due to favorable growing conditions for plants, in particular an increase in rainfall. Based on monthly rainfall satellite data from the Tropical Rainfall Measuring Mission (TRMM), we found
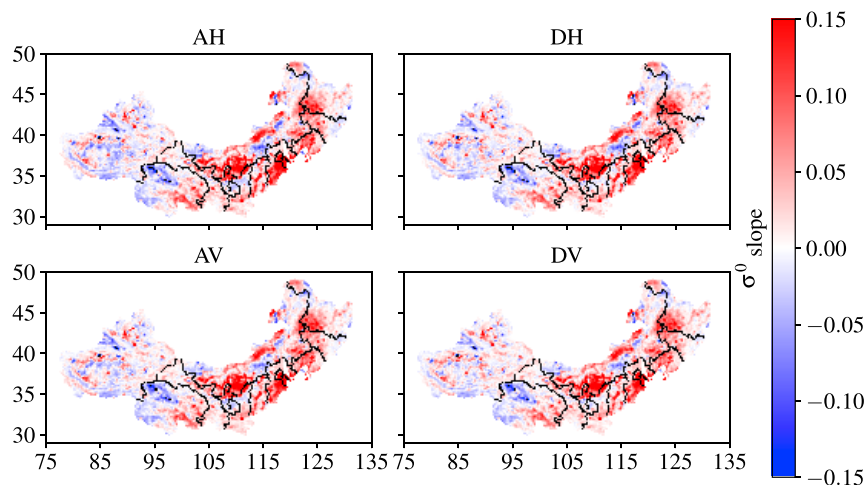
Figure 3. Maps of the Slope (dB/Year) of the Best Linear Fit of the Evolution of QuikSCAT σ^0 between 2000 and 2009

A and D refer to the direction of the satellite during the overpass (ascending or descending) and correspond to different overpass times: ~6 AM, and ~6PM, respectively. V and H refer to the polarization (vertical or horizontal). An increase (decrease) in σ^0 corresponds to an increase (decrease) in vegetation water content that is likely due to an increase (decrease) in vegetation cover. See also Figure S4.

that most of the TNSP area experienced an increase in annual rainfall between 2000 and 2014 (Figure S10). When compared with SIF (Figure 7), we found a positive but non-significant correlation ($R^2 = 0.10$, $p = 0.09$) between the evolution of rainfall over the 2000–2014 period and that of SIF retrievals. In semi-arid ecosystems such as our study region, SIF is expected to be positively correlated with rainfall amount because an increase in soil water content contributes to enhanced photosynthetic activity in temperate and dry ecosystems.[59] However, here the lack of significance suggests that the enhanced vegetation productivity indicated by the positive trend in SIF is driven by a mechanism other than rainfall, likely reforestation efforts. A similar correlation was found when comparing TRMM with σ^0 (Figure S11A, $R^2 = 0.18$, $p = 0.03$). We also compared the slope of the linear regression of the temporal evolution (example in Figure S4) of SIF retrievals and TRMM over latitudinal bands between 30°N and 50°N (corresponding to the area of the TNSP). We found no correlation for the latitudinal bands (see Figure S11B, $p = 0.59$), confirming that the correlation found in Figure 7 was not due to our latitude-dependent correction of the Metop-A data (see section on Solar-Induced Chlorophyll Fluorescence). Finally, we looked at the yearly averaged SIF and σ^0_{DH} signals compared with the mean annual precipitation (Figures S12 and S13 for the TNSP provinces, and Figures S14 and S15 for the sub-provinces of Inner Mongolia). We found that only a few provinces and sub-provinces had a significant correlation between the satellite signal and rainfall amount. This shows that while there is indeed an effect of rainfall on the satellite signal, this effect is limited and cannot account for the integrity of the observed increase in vegetation water content and photosynthetic activity.

Comparison with Optical Remote Sensing Methods

In order to understand what the added value is of SIF and QuikSCAT data over more commonly used optical remote sensing analysis, we looked at the correlation between official planting data and MODIS EVI,[53] an optical/near-infrared (NIR) remote sensing product that quantifies the "greenness" of the surface and is frequently used for land cover change studies.[60] We find that EVI correlates strongly with active reforestation (Figure S16, $R^2 = 0.66$, $p < 0.0001$) but has a weaker correlation

with natural reforestation ($R^2 = 0.45$, $p < 0.001$), indicating that vegetation indices such as EVI are a useful tool to study dense vegetation, as might be the case for active reforestation, but are not as well suited to track the growth of low-greenness vegetation, such as that found in drylands.

DISCUSSION

Implications for Reforestation Efforts in China

Our results show a strong, positive correlation between the extent of the reforested areas and both photosynthetic activity from SIF and canopy water from active microwave remote sensing. The positive trend found in all three datasets indicates that even though the survival rate of trees in reforested areas in the TNSP area is low,[27] there is still a positive effect of reforestation on vegetation activity and wet biomass in the area. In particular, the simultaneous increase in signals captured by GOME-2 and QuikSCAT strongly suggests that vegetation biomass is indeed increasing and that using reforestation as a way to increase ecosystem productivity and decrease desert progression is working. This is especially important because China listed an increase in forest stock as a method to reduce its carbon footprint in its Nationally Determined Contribution (NDC)[61] to the Paris Agreement in 2015. It specifically stated as a goal:[62] "To increase the volume of forest stock by approximately 4.5 cubic meters over 2005 levels."

Here, we showed that dryland reforestation is associated with strong increases in photosynthetic activity (Figure 5) that is itself linked to carbon storage[49] and supports China's claim that reforestation, even in drylands, could potentially be an effective carbon-capture method. Interestingly, we found that afforestation efforts were more successful in the slightly wetter eastern part of the TNSP domain, underscoring the difficulty of long-term afforestation efforts in arid and semi-arid regions, making the need for a reliable, regular monitoring method all the more important.

The increase in vegetation productivity and moisture observed from SIF and QuikSCAT, respectively, may however not be directly correlated with an increase in carbon storage, because vegetation respiration and decomposition of soil organic matter are also changing and might be releasing more CO_2 than the vegetation is taking up. In order to quantify the carbon capture from reforestation for the purpose of meeting China's NDC,
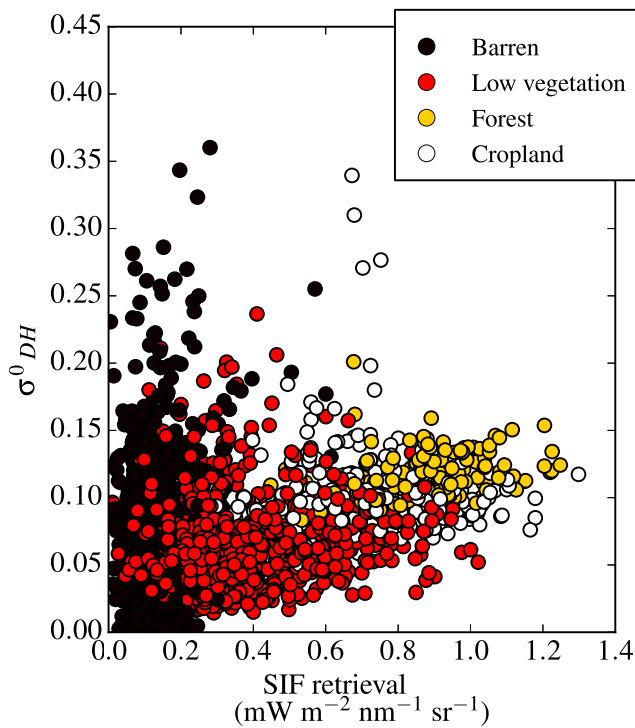
Figure 4. Pixel to Pixel Comparison of SIF and σ^0 for 2009
Markers are color-coded by land use type from MODIS. Similar figures for 2007 and 2008 are available in the Supplemental Information (Figure S9).

doubts about artificial planting, our results indicate that both natural and active reforestation are correlated with increased productivity and increased moist biomass. This is a surprising result, because traditional (active) afforestation efforts in drylands have often been highlighted as a large-scale failure.[27,28,37] One possible explanation for the comparable success of active and natural reforestation is that naturally reforested areas have a slower growth rate than other methods, which leads to a smaller satellite signal. We attempted to take this issue into account in our analysis (see Experimental Procedures), but there is likely still a bias in favor of fast growing, active reforestation methods. In addition, our analysis started when airplane planting was already being phased out by most provinces. Airplane planting is the planting strategy with the lowest level of community engagement,[65] usually leading to a low rate of germination and survival.[38,66] This is in part the reason for the failure of the early phases of the TNSP that relied more heavily on airplane planting. Natural reforestation is encouraged by providing farmers with subsidies or non-agricultural employment opportunities outside the region. Only the analysis of a longer time series and fine-scale planting data can improve the comparison between the different reforestation methods.

Overall, our results are encouraging for natural reforestation efforts. We found that closing land and allowing natural reforestation to recolonize an area is indeed leading to an increase in vegetation cover and activity (Figures 5, 6, and S7). This is especially important because the biodiversity and ecosystem services are much higher for natural reforestation than for planted forests.[38,67] This study is the first time that natural reforestation in China's dryland areas has been clearly identified as being an effective reforestation method that should be encouraged.

There is currently no automatic feedback mechanism between the Chinese State Forest Administration and the scientific community that would allow research progress to be automatically incorporated into future reforestation strategies. However, the State Forest Administration technical committee does include many scientists from the community and is regularly consulted before each new phase of the TNSP. In the past decade, the shift toward environmentally adapted reforestation strategies has been accelerating, driven by a series of studies demonstrating the need for better practices.[68] This is true of the planting method (active versus natural) but also of the species choice. Indeed, the planting data used for this study did not differentiate between different species used for manual planting. However, the manual planting of native shrubs is expected to have a higher success rate than the manual planting of poplars, for example.[69] This shift in species started to occur about a decade ago,[70] and the higher survival rate of native species is just starting to become apparent.

Future Directions for Reforestation Policy Evaluation
Both QuikSCAT and SIF data products are more sensitive to natural reforestation than EVI, likely because natural reforestation tends to have low greenness that is difficult to capture with optical/NIR remote sensing. This indicates that these new types of data have the potential to provide new information regarding dryland reforestation.

The QuikSCAT mission ended in 2009 after a mechanical failure. Other missions have since been launched, such as the Oceansat-2 Scatterometer (OSCAT, ceased to function in
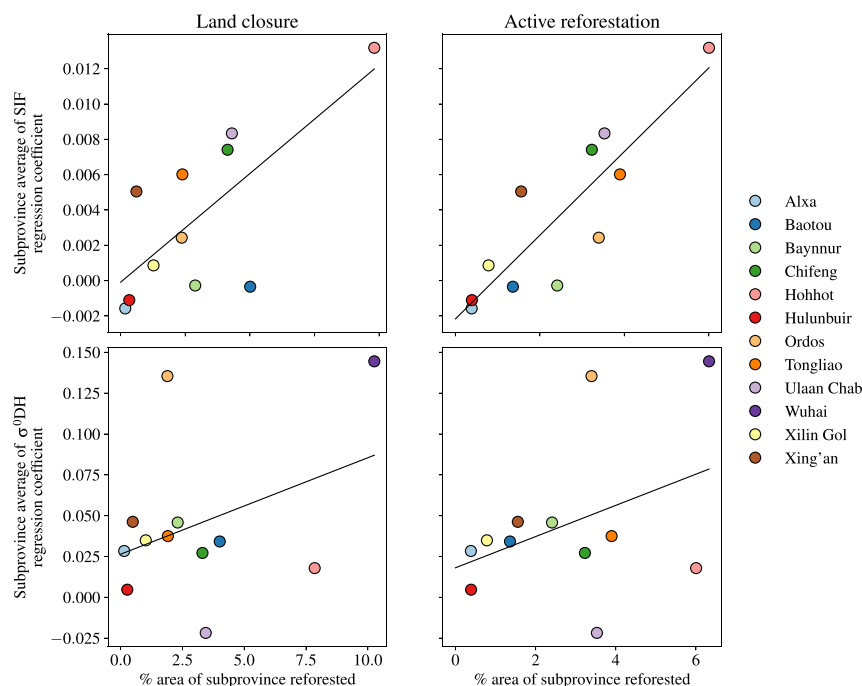
further analysis will be needed. Calibration of SIF retrievals to provide estimates of the amount of CO_2 absorbed by vegetation are slowly becoming available,[63] but SIF signals from dryland ecosystems are understudied, and it is unclear how the retrieved SIF value is quantitatively related to gross carbon uptake for these landscapes. Moreover, the regional net carbon balance would need to be inferred from other data sources, such as remotely sensed atmospheric CO_2 concentrations.[64]

The effect of environmental drivers, in particular rain, cannot be completely untangled from the anthropogenic effects of reforestation on vegetation activity. It might be especially difficult to separate the two, because wetter areas appear to be more extensively planted. For example, in Inner Mongolia, Alxa is the sub-province with the lowest average rainfall (112 mm/year) and the smallest percentage of reforested area (Figure 6), while Hohhot has one of the highest mean annual precipitation in Inner Mongolia (418 mm/year) and also one of the highest rates of reforestation. However, despite this limitation, the link between observed vegetation activity and reforestation (Figures 5 and 6) is stronger than the one observed between vegetation activity and rainfall (Figure 7), indicating that reforestation is likely the driving force behind the increase in vegetation productivity and moisture seen from satellites.

Implications for Reforestation Strategies
We expected to find that natural reforestation was more successful than active reforestation, because the method is better adapted to colonizing difficult ecosystems. However, despite

consistent measurement of dryland vegetation growth, the combination of SIF and active microwave remote sensing will be an excellent method for this purpose.

Conclusion

In this study, we presented two independent types of remote sensing data that offer new insight on reforestation efforts in drylands: microwave remote sensing backscatter provides information on the water status of plants and soil, and SIF is an indirect measure of photosynthesis, which can be used to indicate successful forest regrowth. Looking at the Three-North Shelterbelt Project in Northern China, both techniques show a strong correlation with reforestation data from the Chinese government's Yearbooks, which provide information on the land area reforested using various strategies, but not on the actual effectiveness of the reforestation efforts. We found that, like active reforestation, natural reforestation, i.e., the closing of land to allow natural reforestation to recolonize an area, is strongly correlated with an increase in landscape photosynthesis and vegetation biomass, as intended. This is an important result because natural reforestation has many long-term benefits to the ecosystems that active reforestation might not provide. Future SIF and microwave missions might be able to monitor the success rate of reforestation efforts in drylands in China as well as other areas in the world, for example, the Sahel, where Africa's Great Green Wall is bringing together over 20 countries in the fight against desertification.

2014)[71] launched by the India Space Research Organization in 2009 or the Haiyang-2A (HY-2A) satellite launched in 2011.[72] Finally, ScatSAT was launched in 2016 to replace OSCAT and has already demonstrated its sensitivity to vegetation processes.[73] Since QuikSCAT's failure, these satellites, properly cross-calibrated, have provided a nearly continuous dataset that can be used for near-real-time monitoring of reforestation in drylands, as well as to elucidate longer-term trends. However, the sensitivity of this type of data to both urban growth and soil moisture means that it should be used with caution, especially at fine spatial scale, when the proportion of these effects might be large.

New and improved remotely sensed SIF data recently became available through the TROPOspheric Monitoring Instrument (TROPOMI) launched in October 2017[74] and from TanSat, launched in December 2016.[75] With its global coverage at 7 km × 3.5 km pixels with daily revisit, TROPOMI's temporal and spatial resolutions are much better than other remotely sensed SIF datasets. In addition, the FLuorescence EXplorer (FLEX) mission[76] will be launched by the European Space Agency in 2022. While SIF was only a side product of the GOME-2 and TROPOMI missions, FLEX was designed with the specific purpose of getting high-resolution SIF data (spatial resolution, 0.09 km^2). Combined with emerging models linking SIF retrievals with CO_2 assimilation[63] and a careful cross-calibration with *in situ* measurements, such as tower-mounted PhotoSpec instruments,[77] SIF can provide a metric to monitor reforestation efforts not only in China but also in other crucial regions that are expected to undergo desertification, including the Sahel.[78] Unlike China's Green Great Wall (as the TNSP is often called in the media), which is the work of a single government, Africa's Great Green Wall project brings together more than 20 countries from Sub-Saharan Africa with widely different resources. For the project to succeed, a country-independent method to measure progress will be crucial to hold the different governments accountable.[79,80] By providing globally
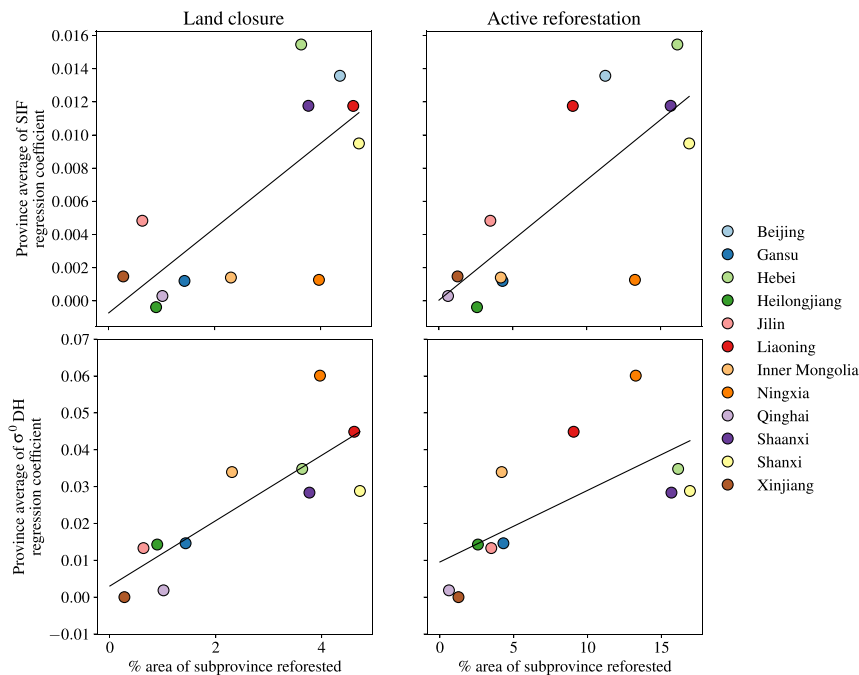
EXPERIMENTAL PROCEDURES

Reforestation Strategies in China

Information on past and current legislation regarding forests in China was obtained from two official sources: (1) the official website of the State Forestry Administration of the People's Republic of China (http://english.forestry.gov.cn/index.php) and (2) the FAOLEX Database (http://www.fao.org/faolex/en/), a database developed by the Food and Agriculture Organization of the United Nations and one of the world's largest electronic collections of national laws, regulations, and policies on food, agriculture, and natural resources management.

The Forest Law of the People's Republic of China, adopted in 1984 and amended in 1998, dedicates Chapter IV to afforestation and states that: "The people's governments at various levels shall work out afforestation plans and, in light of the specific local conditions, set forth targets for increasing the forest coverage of their own areas. People's governments at various levels shall mobilize people of all walks of life and urban and rural inhabitants to fulfill the tasks assigned in the afforestation plans." In 2001, the Law of the People's Republic of

did not implement any natural reforestation over the period of this study. Data from Inner Mongolia separate afforestation data as "artificial" (manual) planting, "airplane" planting, and "land closure" (natural reforestation). Data extracted from the Yearbooks are available in Table S3 in the Supplemental Information.

Microwave Remote Sensing

Active microwave remote sensing provides a proxy for the water content of the surface off which a pulsed microwave signal is backscattered (i.e., reflected) to a detector on board the satellite. For microwave backscattering instruments, the signal analyzed is the backscattering cross-section, σ^0, defined as

$$\sigma^0 = 10\log_{10}\left(\frac{\text{power detected}}{\text{power of the source}}\right), \quad \text{(Equation 1)}$$

where the power detected is the power scattered back to the satellite by the planet's surface.

Here, we use the backscattering cross-section σ^0 of the SeaWinds scatterometer. Launched in 1999 aboard the QuikSCAT satellite, SeaWinds (13.4 GHz, Ku-band, sun-synchronous orbit) has overpass times of 6:00AM (ascending direction, the satellite travels toward the North Pole) and 6:00PM (descending direction, the satellite travels toward the South Pole) around the Equator.[81] QuikSCAT data processed by the NASA Scatterometer Climate Record Pathfinder at Brigham Young University (BYU) offers global coverage every 4 days with a spatial resolution of 4.5 × 4.5 km. The instrument has two beams with different polarizations. In the HH polarization, the electric field vector is perpendicular to the plane of incidence, whereas in the VV polarization, the electric field vector lies in the plane of incidence. The beams in the VV and HH polarizations have incidence angles of 55° and 46°, respectively.[81] Four separate datasets therefore exist for σ^0 from QuikSCAT corresponding to the two overpass times and the two polarizations. In the following, these four datasets are referred to as AV, AH, DV, and DH, where the first letter refers to the direction of the overpass (ascending or descending) and the second letter to the polarization (vertical or horizontal). Because vegetation can be represented as a cloud of randomly oriented leaves, we do not expect any significant difference between the four datasets.

Because of its high dielectric constant, water interacts strongly with microwaves.[82] For this reason, microwave remote sensing is highly sensitive to surface water content, such as soil moisture or plant internal water,[82,83] and at high frequency (approx. 5 GHz and above), can measure changes in total canopy water.[55,84–86] In particular, at QuikSCAT's operating frequency, σ^0 is especially sensitive to the presence of water within the leaves[86,87] and is considered a measure a total vegetation biomass.[55,88]

Data are available on the BYU Microwave Earth Remote Sensing Laboratory website[48] (http://www.mers.byu.edu/). Although the dataset is available from 1999 to 2009, data for 1999 does not encompass a full annual cycle, which might create biases when looking at yearly averages. 2009 is missing the month of December due to instrument failure at the end of November 2009. However, since December is outside the growing season (see

China on Prevention and Control of Desertification was adopted to "prevent land desertification, to transform desertified land, to protect the safety of environment, and to promote the sustainable development of economy and society." Finally, China included reforestation as a way to decrease its carbon emissions in its NDC at the 2015 United Nations Climate Change Conference in Paris.[62] The TNSP, initiated in 1978, is one of the oldest and is the most extensive reforestation project undertaken by the Chinese government. The TNSP spreads across 13 provinces and autonomous regions in Northern China (Figure S1): Heilongjiang, Jilin, Liaoning, Hebei, Shanxi, Shaanxi, Gansu, Qinghai, Tianjin City, Beijing City, Inner Mongolia, Ningxia, and Xinjiang.[23] Here, we set out to investigate how successful efforts at TNSP reforestation have been by comparing official reforestation data reported by the provinces with satellite data.

Reforestation data were obtained using provincial district (provinces or autonomous regions) Yearbooks obtained via the China Statistics Database, Soshoo (http://english.soshoo.com/enindex.do), accessed through the University of Michigan. The search included district names with the words: "land use," "afforestation," or "forest." The level of detail of the available data varied between districts. Yearly afforestation data were only available at the province level. The data used here are available as a separate spreadsheet (Table S3) in the Supplemental Information, and a summary of the available data is presented in Table S2. Detailed information on yearly afforestation efforts at the sub-province level was available only for Inner Mongolia (2006–2010), Liaoning (2000 and 2006–2010), Qinghai (2003–2007), and Xinjiang (2005–2010), but because the four provinces did not provide the same type of information for their sub-provinces, it was not possible to use the data to compare sub-province level patterns. However, since Inner Mongolia is the leader of reforestation efforts within the TNSP (7 million hectares reforested between 2003 and 2015, more than double the area reforested by the second most reforested province), we used the reforestation data from Inner Mongolia as a case study for finer scale data.

Of the 13 provinces included in the Three-North Shelterbelt Project, 12 included "closure of land" for natural reforestation purposes as an afforestation method deployed starting in 2007. For example, the amount of new land closed each year in Xinjiang Province doubled within 4 years. Other reforestation methods included manual and airplane planting (see Table S3 in the Supplemental Information). In 2015, two new categories of reforestation methods were introduced in the Yearbooks: "artificial regeneration" and "restoration of degraded forest." Since 2015 was beyond the time frame of the other datasets we had (see Table S1), we did not consider these two categories separately in our analysis. Tianjin City was excluded from the following analysis because it
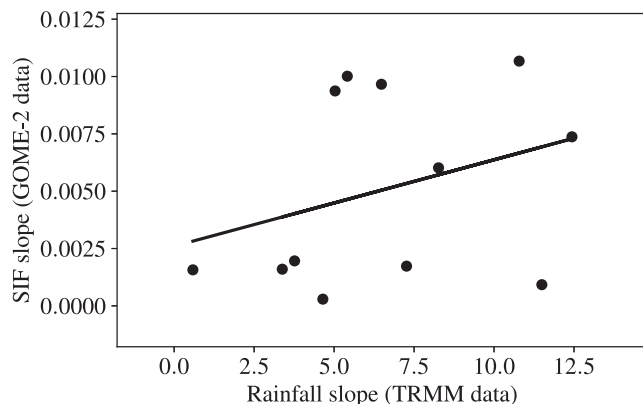
Figure 7. Evolution of SIF and Rainfall
Average slope of the linear regression of the temporal evolution (example in Figure S4) of SIF retrievals for each province as a function of the average slope of the linear regression of the temporal evolution of yearly rainfall from TRMM. The black line shows the best linear regression ($R^2 = 0.10$, $p = 0.09$).

Figure S5), we decided to include 2009 in our analysis and used the years 2000–2009.

Effect of Urban Growth on the Backscatter Signal

Because of the geometry (corner effect) and the construction material of tall buildings, cities and built-up areas have a very strong signal in microwave backscattering.[58] The signal for these areas is much stronger than the signal from natural surfaces. Over the time frame of the QuikSCAT data (2000–2009), China experienced strong urban growth throughout the country.[58,89] To ensure that the signal we analyzed was not affected by changes from natural to urban land cover, we removed pixels from urban areas. To do so, we used the backscatter data from 2008, the last year of our dataset, and the year at which urban extent was the largest. We chose a threshold of $\sigma^0 = -8$ dB as our cutoff, because this is the maximum backscatter signal that has been found for vegetation.[90] The resulting mask is presented in Figure S6 and shows that cities are being effectively masked. In addition, snow-covered areas in the far western part of the TNSP were also masked by this threshold. However, these areas are not being reforested and can therefore be ignored for our purposes.

Solar-Induced Chlorophyll Fluorescence

SIF provides a complementary proxy for vegetation productivity. SIF describes the naturally occurring photon emission by chlorophyll molecules when they drop from an excited to a non-excited state.[49] When a solar photon is absorbed by vegetation chlorophyll, the energy can either be quenched via photochemistry (i.e., photosynthesis) or by re-emission as heat or fluorescence at a red-shifted frequency compared with that of the photon absorbed. Empirically, the dominant pathway for non-photochemical quenching is radiation as heat, meaning that photosynthesis and fluorescence scale with each other, rather than being anti-correlated.[91] While SIF is a broad spectral feature, its influence on infilling narrow spectral features, such as oxygen lines or solar Fraunhofer lines, can be inferred from satellite observations.[50] SIF has been shown to be strongly correlated to other classic vegetation measurements such as satellite enhanced vegetation index[55] or gross primary productivity measured by flux towers.[92]

For this study, we used the monthly SIF data from the Global Ozone Monitoring Experiment 2 (GOME-2) instrument aboard the Metop-A satellite.[93] In particular, we chose to use the Level 3, gridded SIF data with a spatial resolution of $0.5° \times 0.5°$ and referenced to 740 nm from the v2.7 processing,[94] which has improved bias corrections and calibration compared with previous versions. Data from Metop-A was chosen over Metop-B since the former was launched in 2012, whereas Metop-A has been available since 2007. The monthly data were aggregated to yearly level since reforestation data are only available yearly.

Metop-A Temporal Degradation

The GOME-2 instrument aboard Metop-A experienced a degradation in signal in the early years of its operation.[95] This is apparent in the latitudinal average of the SIF retrieval, ρ, calculated as

$$\rho_{lat} = \int_{-180}^{180} SIF_{lat} \, d \, lon, \qquad \text{(Equation 2)}$$

where SIF_{lat} is the SIF measurement at a given latitudinal band. The latitudinal average is expected to stay stable with time. However, when compared with ρ at year 1 of GOME-2's operation, there is a strong drop in signal intensity (Figure S3). This temporal degradation in the signal has been pointed out before,[95] and the interpretation of the Metop-A SIF temporal evolution is not recommended.[96] However, this issue does not affect comparisons of SIF time series between two different locations (J. Joiner, personal communication). In the following, the SIF data are corrected by multiplying each grid cell by the $\rho_{lat}^1/\rho_{lat}^n$ coefficient for the corresponding latitude and year n of the grid cell.

Vegetation Index

We use the MODIS EVI to understand the added value of microwave and SIF remote sensing data over classic "greenness" indices used in previous studies.[9,30,32] Here, we use the monthly MODIS EVI at $0.05° \times 0.05°$ resolution (Product MOD13C2, v.6) available online on NASA's website (https://modis.gsfc.nasa.gov/data/dataprod/mod13.php).

Precipitation and Land Use Type

We analyzed precipitation and land cover data to examine whether trends in the remote sensing data could be due to ancillary factors unrelated to afforestation efforts. For rainfall data, we used the TRMM monthly rainfall estimate L3 V7 with a spatial resolution of $0.25° \times 0.25°$ (TMPA/3B43). The precipitation data are given as the average rainfall rate in millimeters/hour from which we calculated total monthly rainfall, and finally yearly total rainfall. We used data from 2000 to 2014, at which point issues with the spacecraft battery arose, eventually leading to instrument failure in 2015. One of the limitations of TRMM is that its spatial range only extends to 50°N, therefore excluding a small part of Inner Mongolia and Heilongjiang.

We use the Global Mosaics of the standard MODIS land cover type data product (MCD12Q1) to determine and compare the SIF and microwave signals from different land cover types. This dataset has two spatial resolutions, $0.5° \times 0.5°$ and 5×5 min, and was downloaded from the website of the Global Land Cover Facility of the University of Maryland. Land surfaces are divided into the following 17 categories: water bodies, evergreen needleleaf forests, evergreen broadleaf forests, deciduous needleleaf forests, deciduous broadleaf forests, mixed forests, closed shrublands, open shrublands, woody savannas, savannas, grasslands, permanent wetlands, croplands, urban and built-up lands, cropland/natural vegetation mosaics, snow/ice, and barren. For simplicity, we use a single year of data, 2012, the most recent data available. The $0.5° \times 0.5°$ resolution dataset was used to analyze SIF data, and the high-resolution version was used to analyze QuikSCAT and EVI data.

Data Analysis

One complication for our study was that the datasets assembled for our analysis cover different (but overlapping) time periods (see Table S1). Here, we analyzed the temporal evolution of each pixel by calculating the linear regression of each remote sensing dataset (Figure S4) and comparing the slope of each of these. The data were then averaged for each province to match the spatial resolution of the reforestation data. When comparing different remote sensing products, the data were put onto the SIF data grid because it was the dataset with the coarsest resolution.

Agricultural Intensification

Since the early 1990s, the north-east of the TNSP area has been experiencing significant agricultural intensification.[97] Higher agricultural productivity should lead to an increase in both SIF and microwave signals and could bias our results. To remove any potential signal related to agricultural intensification, we masked out pixels identified as cropland in the MODIS land cover product from our analysis of SIF, QuikSCAT, and EVI data.

DATA AND CODE AVAILABILITY

The datasets analyzed in this study are publicly available as referenced within the article. Table S3, provided as a separate Excel file, summarizes the Year-book data used in the study.

SUPPLEMENTAL INFORMATION

Supplemental Information can be found online at https://doi.org/10.1016/j.oneear.2019.12.015.

AUTHOR CONTRIBUTIONS

C.G.-S., F.W., G.K.-A., and D.L.M. designed the study. C.G.-S. acquired the data. C.G.-S., G.K.-A., and S.F. analyzed and interpreted the data. C.G.-S. drafted the manuscript. All authors contributed ideas for analyses, critical revisions, and comments.

DECLARATION OF INTERESTS

The authors declare no competing interests.

REFERENCES

1. Helldén, U., and Tottrup, C. (2008). Regional desertification: a global synthesis. Glob. Planet. Change *64*, 169–176.

2. D'Odorico, P., Bhattachan, A., Davis, K.F., Ravi, S., and Runyan, C.W. (2013). Global desertification: drivers and feedbacks. Adv. Water Resour. *51*, 326–344.

3. Huang, J., Yu, H., Guan, X., Wang, G., and Guo, R. (2016). Accelerated dryland expansion under climate change. Nat. Clim. Change *6*, 166–171.

4. Zhou, W., Gang, C., Zhou, F., Li, J., Dong, X., and Zhao, C. (2015). Quantitative assessment of the individual contribution of climate and human factors to desertification in northwest China using net primary productivity as an indicator. Ecol. Indic. *48*, 560–569.

5. Otterman, J. (1974). Baring high-albedo soils by overgrazing: a hypothesized desertification mechanism. Science *186*, 531–533.

6. Ibáñez, J., Martínez, J., and Schnabel, S. (2007). Desertification due to overgrazing in a dynamic commercial livestock–grass–soil system. Ecol. Model. *205*, 277–288.

7. Wang, Y., Chu, L., Daryanto, S., Wang, L., Lin, J., and Ala, M. (2018). The impact of grazing on seedling patterns in degraded sparse-elm grassland. Land Degrad. Dev. *27*, 3–8.

8. Bestelmeyer, B.T., Okin, G.S., Duniway, M.C., Archer, S.R., Sayre, N.F., Williamson, J.C., and Herrick, J.E. (2015). Desertification, land use, and the transformation of global drylands. Front. Ecol. Environ. *13*, 28–36.

9. Piao, S., Yin, G., Tan, J., Cheng, L., Huang, M., Li, Y., Liu, R., Mao, J., Myneni, R.B., Peng, S., et al. (2015). Detection and attribution of vegetation greening trend in China over the last 30 years. Glob. Change Biol. *21*, 1601–1609.

10. von Hardenberg, J., Meron, E., Shachak, M., and Zarmi, Y. (2001). Diversity of vegetation patterns and desertification. Phys. Rev. Lett. *87*, 273–274.

11. Giannini, A., Biasutti, M., and Verstraete, M.M. (2008). A climate model-based review of drought in the Sahel: desertification, the re-greening and climate change. Glob. Planet. Change *64*, 119–128.

12. Belala, F., Hirche, A., Muller, S.D., Tourki, M., Salamani, M., Grandi, M., Hamouda, T.A., and Boughani, M. (2018). Rainfall patterns of Algerian steppes and the impacts on natural vegetation in the 20th century. J. Arid Land *10*, 561–573.

13. Xue, Z., Qin, Z., Cheng, F., Ding, G., and Li, H. (2017). Quantitative assessment of aeolian desertification dynamics - A case study in north Shanxi of China (1975 to 2015). Sci. Rep. *7*, 10460.

14. Zhang, C.L., Li, Q., Shen, Y.P., Zhou, N., Wang, X.S., Li, J., and Jia, W.R. (2018). Monitoring of aeolian desertification on the Qinghai-Tibet Plateau from the 1970s to 2015 using Landsat images. Sci. Total Environ. *619-620*, 1648–1659.

15. Wang, F., Zhao, X., Gerlein-Safdi, C., Mu, Y., Wang, D., and Lu, Q. (2017). Global sources, emissions, transport and deposition of dust and sand and their effects on the climate and environment: a review. Front. Environ. Sci. Eng. *11*, 12270–12279.

16. Meng, Z., and Lu, B. (2007). Dust events as a risk factor for daily hospitalization for respiratory and cardiovascular diseases in Minqin, China. Atmos. Environ. *41*, 7048–7058.

17. Mu, H., Battsetseg, B., Ito, T.Y., Otani, S., Onishi, K., and Kurozawa, Y. (2011). Health effects of dust storms: subjective eye and respiratory system symptoms in inhabitants in Mongolia. J. Environ. Health *73*, 18–20.

18. Wang, X., Yang, Y., Dong, Z., and Zhang, C. (2009). Responses of dune activity and desertification in China to global warming in the twenty-first century. Glob. Planet. Change *67*, 167–185.

19. Wang, T. (2014). Aeolian desertification and its control in Northern China. Int. Soil Water Conserv. Res. *2*, 34–41.

20. Wang, T. (2004). Progress in sandy desertification research of China. J. Geogr. Sci. *14*, 387–400.

21. Wang, X., Chen, F., and Dong, Z. (2006). The relative role of climatic and human factors in desertification in semiarid China. Glob. Environ. Change *16*, 48–57.

22. Xu, D.Y., Kang, X.W., Zhuang, D.F., and Pan, J.J. (2010). Multi-scale quantitative assessment of the relative roles of climate change and human activities in desertification - a case study of the Ordos Plateau, China. J. Arid Environ. *74*, 498–507.

23. Li, M.M., Liu, A.T., Zou, C.J., Xu, W.D., Shimizu, H., and Wang, K.Y. (2012). An overview of the "Three-North" Shelterbelt project in China. For. Stud. China *14*, 70–79.

24. Tan, M., and Li, X. (2015). Does the Green Great Wall effectively decrease dust storm intensity in China? A study based on NOAA NDVI and weather station data. Land Use Policy *43*, 42–47.

25. Zhang, Y., Peng, C., Li, W., Tian, L., Zhu, Q., Chen, H., Fang, X., Zhang, G., Liu, G., Mu, X., et al. (2016). Multiple afforestation programs accelerate the greenness in the 'Three North' region of China from 1982 to 2013. Ecol. Indic. *61* (Part 2), 404–412.

26. Niu, Q., Xiao, X., Zhang, Y., Qin, Y., Dang, X., Wang, J., Zou, Z., Doughty, R.B., Brandt, M., Tong, X., et al. (2019). Ecological engineering projects increased vegetation cover, production, and biomass in semiarid and subhumid Northern China. Land Degrad. Dev. *30*, 1620–1631.

27. Cao, S. (2008). Why large-scale afforestation efforts in China have failed to solve the desertification problem. Environ. Sci. Technol. *42*, 1826–1831.

28. Ahrends, A., Hollingsworth, P.M., Beckschäfer, P., Chen, H., Zomer, R.J., Zhang, L., Wang, M., and Xu, J. (2017). China's fight to halt tree cover loss. Proc. Biol. Sci. *284*, 20162559.

29. Duan, H., Yan, C., Tsunekawa, A., Song, X., Li, S., and Xie, J. (2011). Assessing vegetation dynamics in the Three-North Shelter Forest region of China using AVHRR NDVI data. Environ. Earth Sci. *64*, 1011–1020.

30. Wang, F., Pan, X., Gerlein-Safdi, C., Cao, X., Wang, S., Gu, L., Wang, D., and Lu, Q. (2019). Vegetation restoration in Northern China: a contrasted picture. Land Degrad. Dev. *351*, 120–128.

31. Collado, A.D., Chuvieco, E., and Camarasa, A. (2002). Satellite remote sensing analysis to monitor desertification processes in the crop-rangeland boundary of Argentina. J. Arid Environ. *52*, 121–133.

32. Higginbottom, T., and Symeonakis, E. (2014). Assessing land degradation and desertification using vegetation index data: current frameworks and future directions. Remote Sens. *6*, 9552–9575.

33. Zheng, X., Zhu, J.J., Yan, Q.L., and Song, L.N. (2012). Effects of land use changes on the groundwater table and the decline of *Pinus sylvestris* var. *mongolica* plantations in southern Horqin Sandy Land, Northeast China. Agric. Water Manag. *109*, 94–106.

34. Guo, J., Gong, X., Fang, L., Jiang, D., Ala, M., Bucci, S.J., Scholz, F.G., Goldstein, G., and Hao, G.Y. (2019). Switching of dominant positions between two sand-fixing shrub species during the dune revegetation process is underlain by their contrasting xylem hydraulics and water use strategies. Land Degrad. Dev. https://doi.org/10.1002/ldr.3493.

35. Luo, L., Zhuang, Y., Zhao, W., Duan, Q., and Wang, L. (2019). The hidden costs of desert development. Ambio. https://doi.org/10.1007/s13280-019-01287-7.

36. Duan, Z., Honglang, X., Xinrong, L., Zhibao, D., and Gang, W. (2004). Evolution of soil properties on stabilized sands in the Tengger Desert, China. Geomorphology *59*, 237–246.

37. Cao, S., Chen, L., Shankman, D., Wang, C., Wang, X., and Zhang, H. (2011). Excessive reliance on afforestation in China's arid and semi-arid regions: lessons in ecological restoration. Earth Sci. Rev. *104*, 240–245.

38. Chazdon, R.L. (2008). Beyond deforestation: restoring forests and ecosystem services on degraded lands. Science *320*, 1458–1460.

39. Osborne, S. (2018). China reassigns 60,000 soldiers to plant trees in bid to fight pollution. The Independent https://www.independent.co.uk/news/world/asia/china-tree-plant-soldiers-reassign-climate-change-global-warming-deforestation-a8208836.html.

40. Chen, Y., Wang, K., Lin, Y., Shi, W., Song, Y., and He, X. (2015). Balancing green and grain trade. Nat. Geosci. *8*, 739–741.

41. Vina, A., McConnell, W.J., Yang, H., Xu, Z., and Liu, J. (2016). Effects of conservation policy on Chinas forest recovery. Sci. Adv. *2*, e1500965.

42. Tong, X., Brandt, M., Yue, Y., Horion, S., Wang, K., De Keersmaecker, W., Tian, F., Schurgers, G., Xiao, X., Luo, Y., et al. (2018). Increased vegetation growth and carbon stock in China karst via ecological engineering. Nat. Sustain. *1*, 44–50.

43. Chen, C., Park, T., Wang, X., Piao, S., Xu, B., Chaturvedi, R.K., Fuchs, R., Brovkin, V., Ciais, P., Fensholt, R., et al. (2019). China and India lead in greening of the world through land-use management. Nat. Sustain. *2*, 122–129.

44. Ci, L., and Yang, X. (2011). Desertification and its Control in China (Springer).

45. Li, J., Yang, X., Jin, Y., Yang, Z., Huang, W., Zhao, L., Gao, T., Yu, H., Ma, H., Qin, Z., et al. (2013). Monitoring and analysis of grassland desertification dynamics using Landsat images in Ningxia, China. Remote Sens. Environ. *138*, 19–26.

46. Helldén, U.A. (2008). Coupled human-environment model for desertification simulation and impact studies. Glob. Planet. Change *64*, 158–168.

47. Martínez-Valderrama, J., Ibáñez, J., Del Barrio, G., Sanjuán, M.E., Alcalá, F.J., Martínez-Vicente, S., Ruiz, A., and Puigdefábregas, J. (2016). Present and future of desertification in Spain: implementation of a surveillance system to prevent land degradation. Sci. Total Environ. *563-564*, 169–178.

48. Long, D.G., Drinkwater, M.R., Holt, B., Saatchi, S., and Bertoia, C. (2001). Global ice and land climate studies using scatterometer image data. Eos *82*, 503.

49. Porcar-Castell, A., Tyystjärvi, E., Atherton, J., van der Tol, C., Flexas, J., Pfündel, E.E., Moreno, J., Frankenberg, C., and Berry, J.A. (2014). Linking chlorophyll a fluorescence to photosynthesis for remote sensing applications: mechanisms and challenges. J. Exp. Bot. *65*, 4065–4095.

50. Joiner, J., Guanter, L., Lindstrot, R., Voigt, M., Vasilkov, A.P., Middleton, E.M., Huemmrich, K.F., Yoshida, Y., and Frankenberg, C. (2013). Global monitoring of terrestrial chlorophyll fluorescence from moderate-spectral-resolution near-infrared satellite measurements: methodology, simulations, and application to GOME-2. Atmos. Meas. Tech. *6*, 2803–2823.

51. Joiner, J., Yoshida, Y., Vasilkov, A.P., Schaefer, K., Jung, M., Guanter, L., Zhang, Y., Garrity, S., Middleton, E.M., Huemmrich, K.F., et al. (2014). The seasonal cycle of satellite chlorophyll fluorescence observations and its relationship to vegetation phenology and ecosystem atmosphere carbon exchange. Remote Sens. Environ. *152*, 375–391.

52. National Bureau of Statistics of China. (2015). China Statistical Yearbooks, Years 2003 to 2015 (China Statistics Press).

53. Huete, A., Didan, K., Miura, T., Rodriguez, E.P., Gao, X., and Ferreira, L.G. (2002). Overview of the radiometric and biophysical performance of the MODIS vegetation indices. Remote Sens. Environ. *83*, 195–213.

54. National Bureau of Statistics of China. (2010). Inner Mongolia Statistical Yearbooks, Years 2006 to 2010 (China Statistics Press).

55. Guan, K., Wu, J., Kimball, J.S., Anderson, M.C., Frolking, S., Li, B., Hain, C.R., and Lobell, D.B. (2017). The shared and unique values of optical, fluorescence, thermal and microwave satellite data for estimating large-scale crop yields. Remote Sens. Environ. *199*, 333–349.

56. Liu, P.W., Judge, J., DeRoo, R.D., England, A.W., Bongiovanni, T., and Luke, A. (2016). Dominant backscattering mechanisms at L-band during dynamic soil moisture conditions for sandy soils. Remote Sens. Environ. *178*, 104–112.

57. Kolassa, J., Reichle, R.H., and Draper, C.S. (2017). Merging active and passive microwave observations in soil moisture data assimilation. Remote Sens. Environ. *191*, 117–130.

58. Frolking, S., Milliman, T., Seto, K.C., and Friedl, M.A. (2013). A global fingerprint of macro-scale changes in urban structure from 1999 to 2009. Environ. Res. Lett. *8*, 024004.

59. Sun, Y., Fu, R., Dickinson, R., Joiner, J., Frankenberg, C., Gu, L., Xia, Y., and Fernando, N. (2015). Drought onset mechanisms revealed by satellite solar-induced chlorophyll fluorescence: insights from two contrasting extreme events. J. Geophys. Res. Biogeosci. *120*, 2427–2440.

60. Ferreira, N.C., Ferreira, L.G., and Huete, A.R. (2010). Assessing the response of the MODIS vegetation indices to landscape disturbance in the forested areas of the legal Brazilian Amazon. Int. J. Remote Sens. *31*, 745–759.

61. den Elzen, M., Fekete, H., Höhne, N., Admiraal, A., Forsell, N., Hof, A.F., Olivier, J.G., Roelfsema, M., and van Soest, H. (2016). Greenhouse gas emissions from current and enhanced policies of China until 2030: can emissions peak before 2030? Energy Policy *89*, 224–236.

62. Sha, F., Ji, Z., and Linwei, L. (2015). An Analysis of China's INDC (China National Center for Climate Change Strategy and International Cooperation (NCSC)).

63. Zhang, Y., Joiner, J., Alemohammad, S.H., Zhou, S., and Gentine, P. (2018). A global spatially Continuous Solar Induced Fluorescence (CSIF) dataset using neural networks. Biogeosciences *15*, 5779–5800.

64. Keppel-Aleks, G., Wennberg, P.O., O'Dell, C.W., and Wunch, D. (2013). Towards constraints on fossil fuel emissions from total column carbon dioxide. Atmos. Chem. Phys. *13*, 4349–4357.

65. Salvati, L., Kosmas, C., Kairis, O., Karavitis, C., Acikalin, S., Belgacem, A., Solé-Benet, A., Chaker, M., Fassouli, V., Gokceoglu, C., et al. (2016). Assessing the effectiveness of sustainable land management policies for combating desertification: a data mining approach. J. Environ. Manage. *183* (Part 3), 754–762.

66. A. Mather, ed. (1993). Afforestation: Policies, Planning and Progress (Bellhaven Press).

67. Li, F.R., Zhang, H., Zhao, L.Y., Shirato, Y., and Wang, X.Z. (2003). Pedoecological effects of a sand-fixing poplar (*Populus simonii* Carr.) forest in a desertified sandy land of Inner Mongolia, China. Plant Soil *256*, 431–442.

68. Li, W. (2004). Degradation and restoration of forest ecosystems in China. For. Ecol. Manag. *201*, 33–41.

69. Hu, Y.L., Zeng, D.H., Fan, Z.P., Chen, G.S., Zhao, Q., and Pepper, D. (2008). Changes in ecosystem carbon stocks following grassland afforestation of semiarid sandy soil in the southeastern Keerqin Sandy Lands, China. J. Arid Environ. *72*, 2193–2200.

70. Yang, X., and Ci, L. (2008). Comment on "Why large-scale afforestation efforts in China have failed to solve the desertification problem". Environ. Sci. Technol. *42*, 7722–7723.

71. Jaruwatanadilok, S., Stiles, B.W., and Fore, A.G. (2014). Cross-calibration between QuikSCAT and Oceansat-2. IEEE Trans. Geosci. Remote Sens. *52*, 6197–6204.

72. Yang, X., Liu, G., Li, Z., and Yu, Y. (2014). Preliminary validation of ocean surface vector winds estimated from China's HY-2A scatterometer. Int. J. Remote Sens. *35*, 4532–4543.

73. Palakuru, M., Yarrakula, K., Chaube, N.R., Sk, K.B., and Satyaji Rao, Y.R. (2019). Identification of paddy crop phenological parameters using dual polarized SCATSAT-1 (ISRO, India) scatterometer data. Environ. Sci. Pollut. Res. Int. *26*, 1565–1575.

74. Köhler, P., Frankenberg, C., Magney, T.S., Guanter, L., Joiner, J., and Landgraf, J. (2018). Global retrievals of solar-induced chlorophyll fluorescence with TROPOMI: first results and intersensor comparison to OCO-2. Geophys. Res. Lett. *45*, 10456–10463.

75. Du, S., Liu, L., Liu, X., Zhang, X., Zhang, X., Bi, Y., and Zhang, L. (2018). Retrieval of global terrestrial solar-induced chlorophyll fluorescence from TanSat satellite. Sci. Bull. *63*, 1502–1512.

76. Drusch, M., Moreno, J., Del Bello, U., Franco, R., Goulas, Y., Huth, A., Kraft, S., Middleton, E.M., Miglietta, F., Mohammed, G., et al. (2017). The FLuorescence EXplorer Mission Concept—ESA's Earth Explorer 8. IEEE Trans. Geosci. Remote Sens. *55*, 1273–1284.

77. Grossmann, K., Frankenberg, C., Magney, T.S., Hurlock, S.C., Seibt, U., and Stutz, J. (2018). PhotoSpec: a new instrument to measure spatially distributed red and far-red solar-induced chlorophyll fluorescence. Remote Sens. Environ. *216*, 311–327.

78. FAO (2017). Great Green Wall for the Sahara and the Sahel Initiative: The African Wall (Food and Agriculture Organization of the United Nations).

79. Seely, M., Dirkx, E., Hager, C., Klintenberg, P., Roberts, C., and von Oertzen, D. (2008). Advances in desertification and climate change research: are they accessible for application to enhance adaptive capacity? Glob. Planet. Change *64*, 236–243.

80. Verstraete, M.M., Brink, A.B., Scholes, R.J., Beniston, M., and Smith, M.S. (2008). Climate change and desertification: where do we stand, where should we go? Glob. Planet. Change *64*, 105–110.

81. Paget, A.C., Long, D.G., and Madsen, N.M. (2016). RapidScat diurnal cycles over land. IEEE Trans. Geosci. Remote Sens. *54*, 3336–3344.

82. El-Rayes, M.A., and Ulaby, F.T. (1987). Microwave dielectric spectrum of vegetation – Part I: experimental observations. IEEE Trans. Geosci. Remote Sens. *25*, 541–549.

83. Ulaby, F.T., and El-Rayes, M.A. (1987). Microwave dielectric spectrum of vegetation – Part II: dual-dispersion model. IEEE Trans. Geosci. Remote Sens. *25*, 550–557.

84. Satake, M., and Hanado, H. (2004). Diurnal change of Amazon rain forest σ^0 observed by Ku-band spaceborne radar. IEEE Trans. Geosci. Remote Sens. *42*, 1127–1134.

85. Frolking, S., Milliman, T., Palace, M., Wisser, D., Lammers, R., and Fahnestock, M. (2011). Tropical forest backscatter anomaly evident in SeaWinds scatterometer morning overpass data during 2005 drought in Amazonia. Remote Sens. Environ. *115*, 897–907.

86. Steele-Dunne, S.C., Friesen, J., and van de Giesen, N. (2012). Using diurnal variation in backscatter to detect vegetation water stress. IEEE Trans. Geosci. Remote Sens. *50*, 2618–2629.

87. van Emmerik, T., Steele-Dunne, S., Paget, A., Oliveira, R.S., Bittencourt, P.R., Barros, F.D.V., and van de Giesen, N. (2017). Water stress detection in the Amazon using radar. Geophys. Res. Lett. *50*, 6941–6849.

88. Frolking, S., Fahnestock, M., Milliman, T., McDonald, K., and Kimball, J. (2005). Interannual variability in North American grassland biomass/productivity detected by SeaWinds scatterometer backscatter. Geophys. Res. Lett. *32*, L21409.

89. Jacobson, M.Z., Nghiem, S.V., Sorichetta, A., and Whitney, N. (2015). Ring of impact from the mega-urbanization of Beijing between 2000 and 2009. J. Geophys. Res. Atmos. *120*, 5740–5756.

90. Frolking, S., Milliman, T., McDonald, K., Kimball, J., Zhao, M., and Fahnestock, M. (2006). Evaluation of the SeaWinds scatterometer for regional monitoring of vegetation phenology. J. Geophys. Res. *111*, D17302.

91. van der Tol, C., Verhoef, W., and Rosema, A. (2009). A model for chlorophyll fluorescence and photosynthesis at leaf scale. Agric. For. Meteorol. *149*, 96–105.

92. Sun, Y., Frankenberg, C., Wood, J.D., Schimel, D.S., Jung, M., Guanter, L., Drewry, D.T., Verma, M., Porcar-Castell, A., Griffis, T.J., et al. (2017). OCO-2 advances photosynthesis observation from space via solar-induced chlorophyll fluorescence. Science *358*, eaam5747.

93. Munro, R., Lang, R., Klaes, D., Poli, G., Retscher, C., Lindstrot, R., Huckle, R., Lacan, A., Grzegorski, M., Holdak, A., et al. (2016). The GOME-2 instrument on the Metop series of satellites: instrument design, calibration, and level 1 data processing – an overview. Atmos. Meas. Tech. *9*, 1279–1301.

94. Joiner, J., Yoshida, Y., Guanter, L., and Middleton, E.M. (2016). New methods for the retrieval of chlorophyll red fluorescence from hyperspectral satellite instruments: simulations and application to GOME-2 and SCIAMACHY. Atmos. Meas. Tech. *9*, 3939–3967.

95. Sanders, A., Verstraeten, W., Kooreman, M., van Leth, T., Beringer, J., and Joiner, J. (2016). Spaceborne sun-induced vegetation fluorescence time series from 2007 to 2015 evaluated with Australian flux tower measurements. Remote Sens. *8*, 895.

96. Zhang, Y., Joiner, J., Gentine, P., and Zhou, S. (2018). Reduced solar-induced chlorophyll fluorescence from GOME-2 during Amazon drought caused by dataset artifacts. Glob. Change Biol. *24*, 2229–2230.

97. Zuo, L., Zhang, Z., Carlson, K.M., MacDonald, G.K., Brauman, K.A., Liu, Y., Zhang, W., Zhang, H., Wu, W., Zhao, X., et al. (2018). Progress towards sustainable intensification in China challenged by land-use change. Nat. Sustain. *1*, 304–313.

Supplemental Information

Satellite Monitoring of Natural

Reforestation Efforts in China's Drylands

Cynthia Gerlein-Safdi, Gretchen Keppel-Aleks, Feng Wang, Steve Frolking, and Denise L. Mauzerall

Supplemental Information

Satellite monitoring of natural reforestation efforts
in China's drylands

Cynthia Gerlein-Safdi, Gretchen Keppel-Aleks, Feng Wang, Steve Frolking, Denise Mauzerall

Dataset	Source	Years used	Spatial resolution
Afforestation data (China)	China Statistics Database	2003–2015	Province level
Afforestation data (Inner Mongolia)	China Statistics Database	2006–2010	Sub-province level
σ^0 (canopy moisture)	QuikSCAT	2000–2009	4.5×4.5 km
SIF (photosynthetic activity)	GOME-2	2007–2017	$0.5^{\circ} \times 0.5^{\circ}$
Rainfall	TRMM	2000–2014	$0.25^{\circ} \times 0.25^{\circ}$
EVI (vegetation index)	MODIS	2000–2013	$0.05^{\circ} \times 0.05^{\circ}$
Land cover type	MODIS	2012	$0.5^{\circ} \times 0.5^{\circ}$
Land cover type	MODIS	2012	$5' \times 5'$

Table S1: *Summary of the different datasets used for this study with their temporal range and spatial resolution.*

	Total area (km^2)	Type of data available	Spatial scale	Years of data available
Beijing City	16,411	Afforestation area by method and forest function	Province	2003-2015
Gansu	454,430	Afforestation area by method and forest function	Province	2003-2015
Hebei	187,700	Afforestation area by method and forest function	Province	2003-2015
Heilongjiang	454,800	Afforestation area by method and forest function	Province	2003-2015
Inner Mongolia	1,183,000	Afforestation area by method	Sub-province	2006-2010
		Afforestation area by method and forest function	Province	2003-2015
Jilin	191,126	Afforestation area by method and forest function	Province	2003-2015
Liaoning	145,900	Afforestation area by forest function	Sub-province	2000, 2006-2010
		Afforestation area by method and forest function	Province	2003-2015
Ningxia	66,399	Afforestation area by method and forest function	Province	2003-2015
Qinghai	720,000	Afforestation area by forest function	Sub-province	2003-2007
		Afforestation area by method and forest function	Province	2003-2015
Shaanxi	205,800	Afforestation area by method and forest function	Province	2003-2015
Shanxi	156,000	Afforestation area by method and forest function	Province	2003-2015
Tianjin City	11,760	Afforestation area by method and forest function	Province	2003-2015
Xinjiang	1,664,897	Afforestation area by method and forest function	Sub-province	2005-2010
		Afforestation area by method and forest function	Province	2003-2015

Table S2: *Available information on reforestation from the yearbooks for each of the 13 provinces and autonomous regions included within the Three-North Shelterbelt Project Area.*

Table S3: *Excel table (available in a separate file) summarizing the province-level afforestation data available in the Yearbooks from 2003 to 2015. Blue columns are the 13 provinces and autonomous regions that are included in the Three-North Shelterbelt Project. The second tab presents sub-province level reforestation data for Inner Mongolia from 2006 to 2010.*
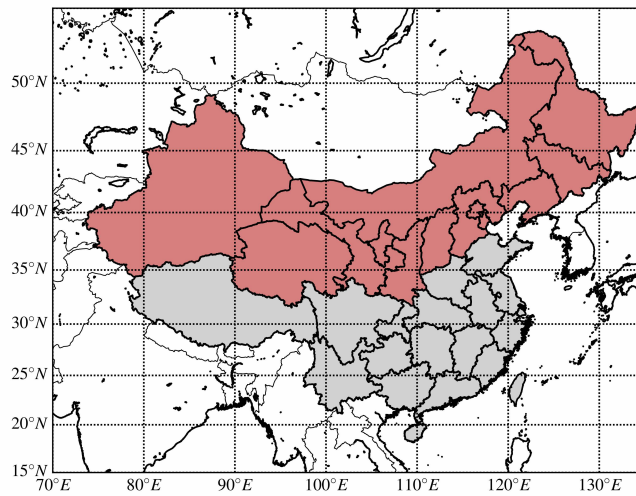
Figure S1: *Map of China showing in red the 13 provinces involved in the Three-North Shelterbelt Project (TNSP): Heilongjiang, Jilin, Liaoning, Hebei, Shanxi, Shaanxi, Gansu, Qinghai, Tianjin City, Beijing City, Inner Mongolia, Ningxia, and Xinjiang. All other figures only show the TNSP area.*
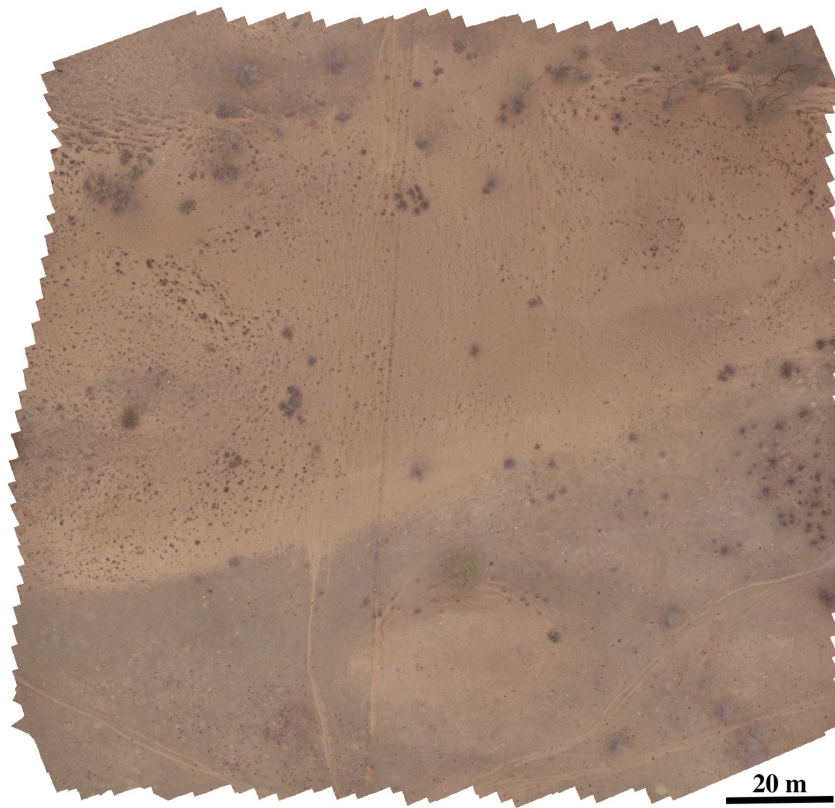

Figure S2: *Bird's eye view (RGB composite image) of a natural reforestation site in Inner Mongolia (42°57'N, 115°57'E) captured by drone . The image was captured in May, at the beginning at the growing season. Although fully grown oak trees are present in the image, their small leaves and thin canopy does not lead to identifiable "greenness" that could be captured by optical remote sensing.*
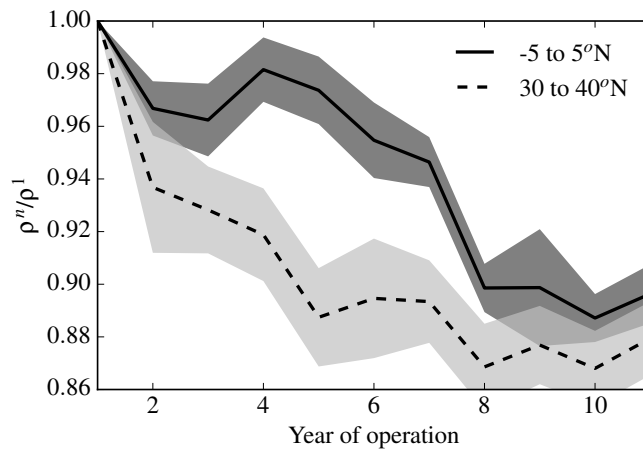
Figure S3: *Latitudinal average throughout GOME-2 lifetime compared to the latitudinal average at Year 1 for two different latitudinal bands. Grey bands show the standard deviation. Here we show the latitudinal average at the Equator between -5 and 5°N (solid line, dark grey band) and between 30 and 40°N, the range of the TNSP area (dashed line, light grey band).*
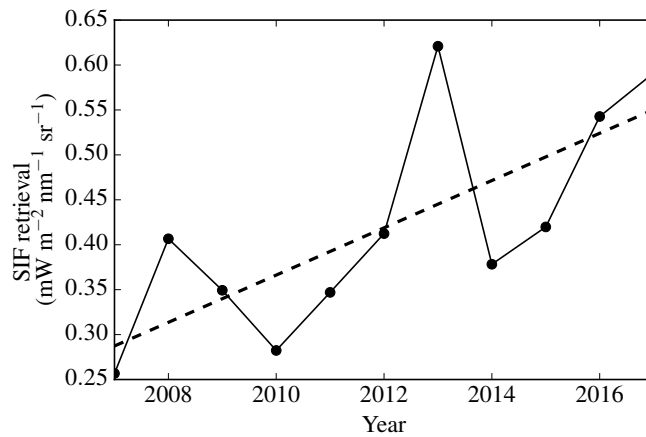
Figure S4: *Temporal evolution of a single SIF pixel within the TNSP area after correction for the latitudinally averaged degradation. The dotted line represents the linear regression. In this specific case, the slope of the linear regression is 0.026 with an R^2 of 0.54.*
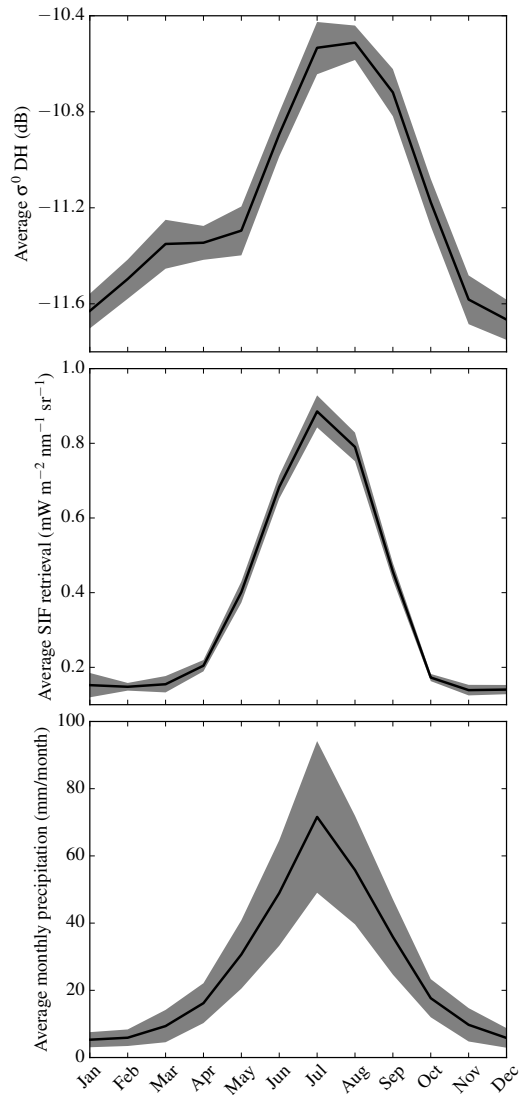
Figure S5: *Monthly average of the backscatter from QuikSCAT (top), the SIF retrievals (center), and the precipitation from TRMM (bottom), averaged for the whole TNSP area over their respective range of operation (see Table S1). Grey bands show the standard deviation.*
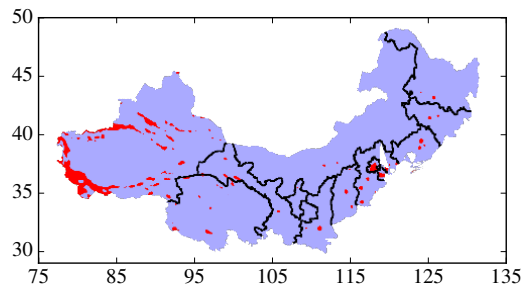
Figure S6: *Mask of σ^0 in the TNSP area in which cities have been masked using a -8 dB threshold and are shown in red. The thresholding also masks snow-covered areas in the far west of the study zone, but these areas are not being reforested and can therefore be ignored here.*

5
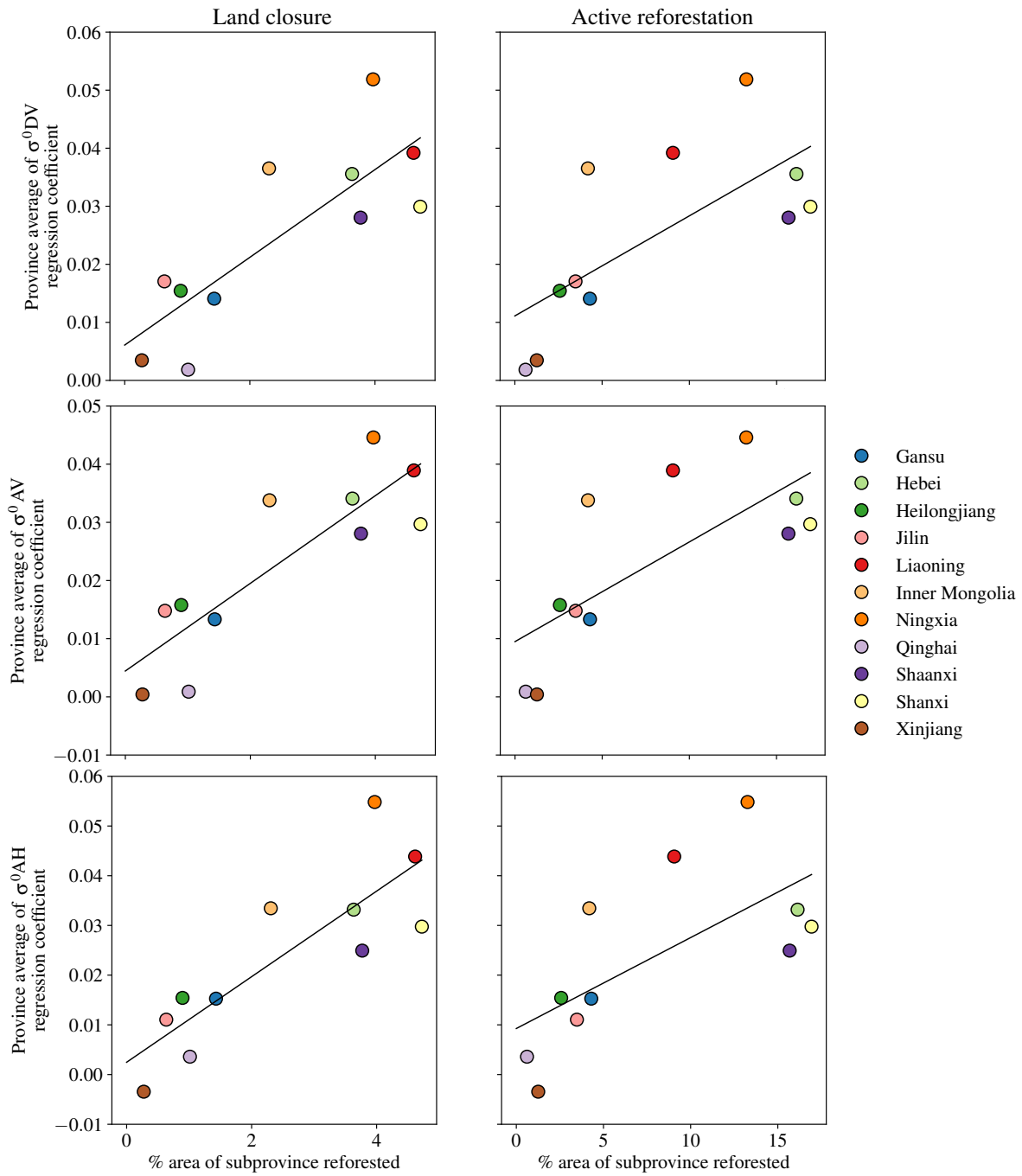
Figure S7: *Average slopes for σ_{DV}^0 (top), σ_{AV}^0 (center), and σ_{AH}^0 (bottom) for each province as a function of the percentage of the province reforested by 1) land closure (left), 2) active reforestation (right). Lines show the best linear regression in each case. Land closure: $R^2 = 0.66$, $R^2 = 0.73$, $R^2 = 0.70$, all with $p < 0.001$ for σ_{DV}^0, σ_{AV}^0, and σ_{AH}^0, respectively. Active reforestation: $R^2 = 0.49$, $R^2 = 0.54$, $R^2 = 0.45$, all with $p < 0.001$. Note that Beijing city was removed from the analysis because of the very high σ^0 likely due to the limited amount of non-urban area and the strong effect of urban development on QuikSCAT data.*
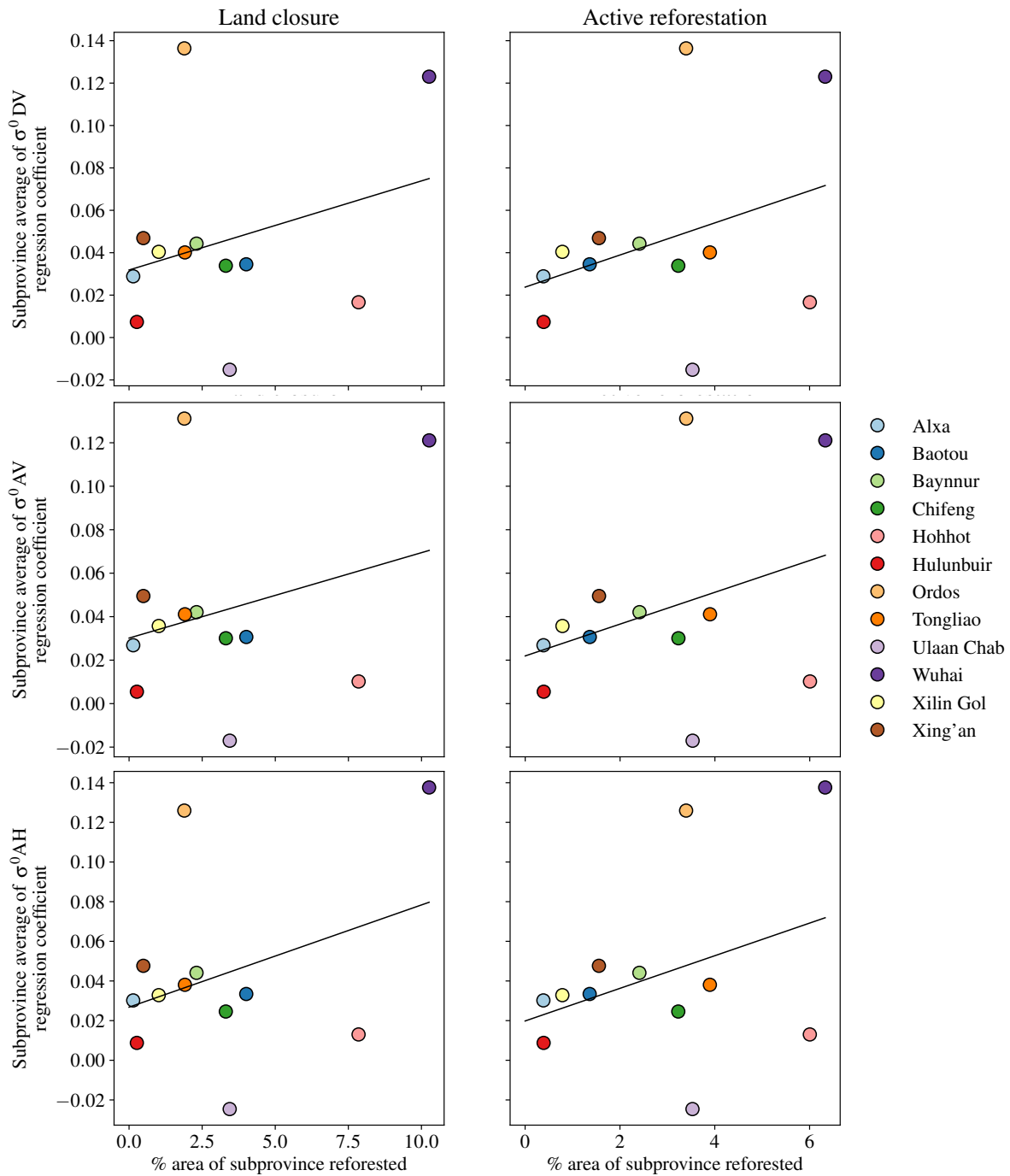
Figure S8: *Average slopes for σ^0_{DV} (top), σ^0_{AV} (center), and σ^0_{AH} (bottom) for each sub-province of Inner Mongolia as a function of the percentage of the sub-province reforested by 1) land closure (left), 2) active reforestation (right). Lines show the best linear regression in each case. Land closure: $R^2 = 0.090$, $p = 0.1$; $R^2 = 0.08$, $p = 0.14$; $R^2 = 0.12$, $p = 0.07$ for σ^0_{DV}, σ^0_{AV}, and σ^0_{AH}, respectively. Active reforestation: $R^2 = 0.12$, $p = 0.07$; $R^2 = 0.12$, $p = 0.07$; $R^2 = 0.13$, $p = 0.06$.*
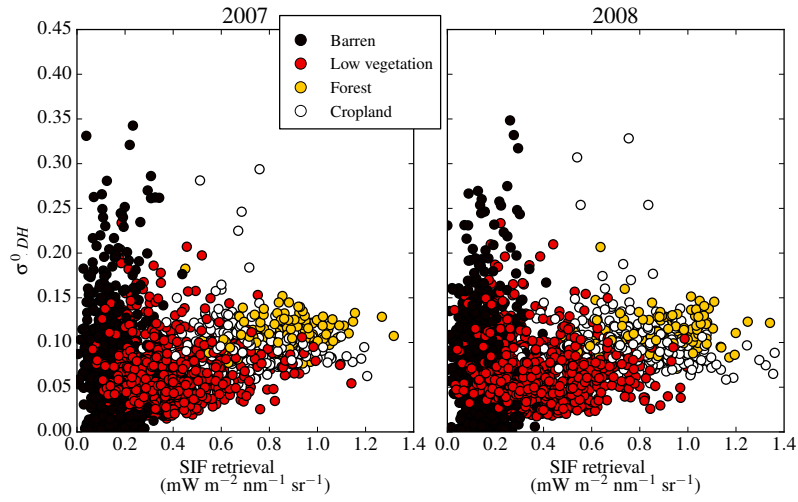
Figure S9: *Pixel to pixel comparison of SIF and σ^0 for the years 2007 and 2008 with markers color-coded by land use type from MODIS. Figure 4 presents a similar figure for the year 2009.*
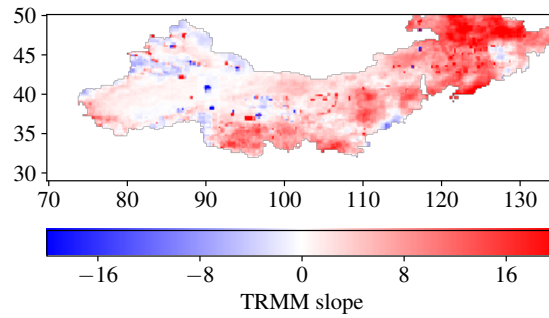
Figure S10: *Map of the slope (mm/year) for the best linear fit of the evolution of rainfall retrievals from TRMM between 2000 and 2014 over the TNSP area.*
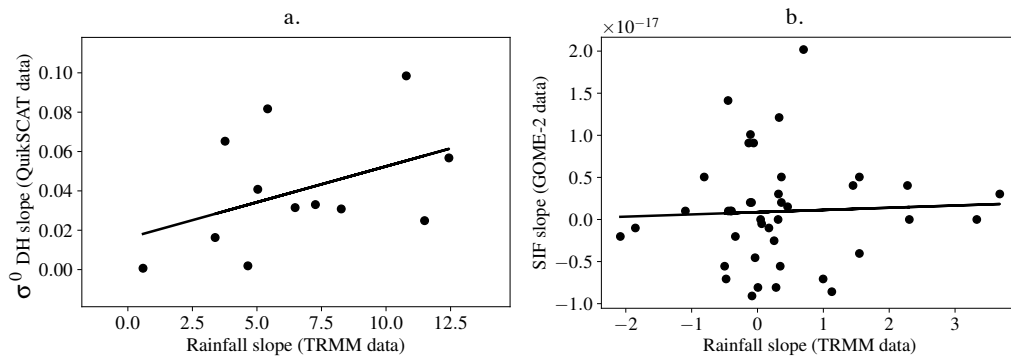

Figure S11: Left: *Average σ^0_{DH} slope for each province as a function of average rainfall coefficient.* **Right:** *Average SIF slope for latitudinal bands between 50^oN and 30^oN as a function of average rainfall coefficient. No significant correlation is found.*
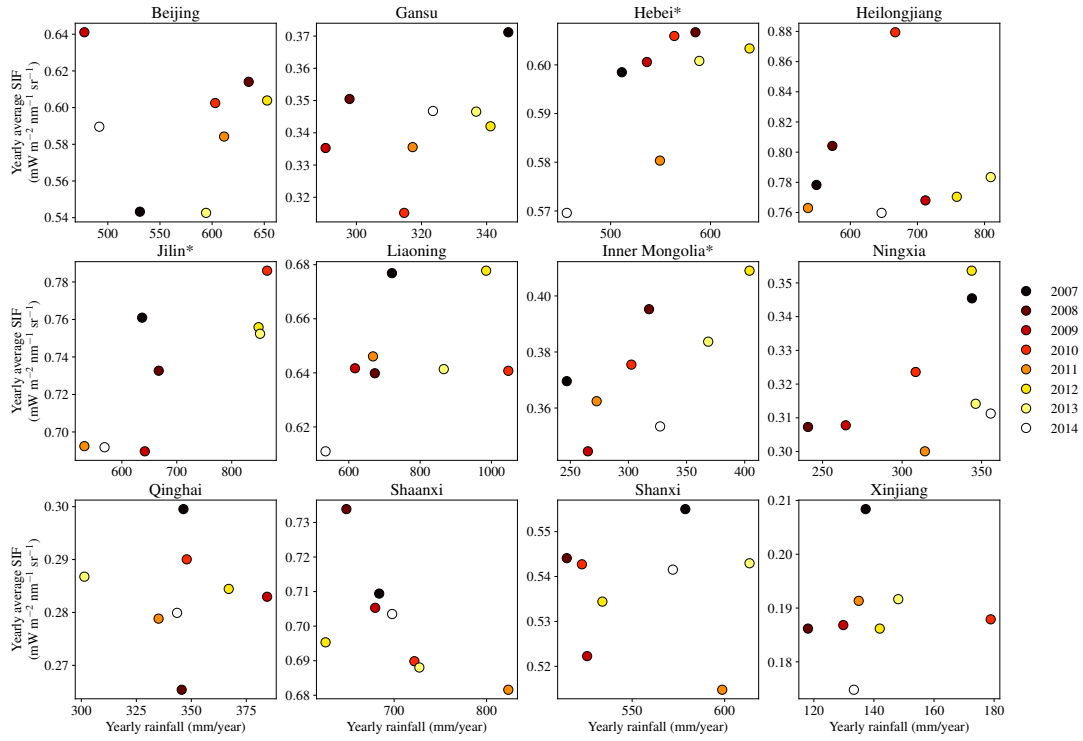
Figure S12: *Yearly average SIF signal as a function of yearly rainfall for each province in the TNSP. '*' indicates a significant correlation.*
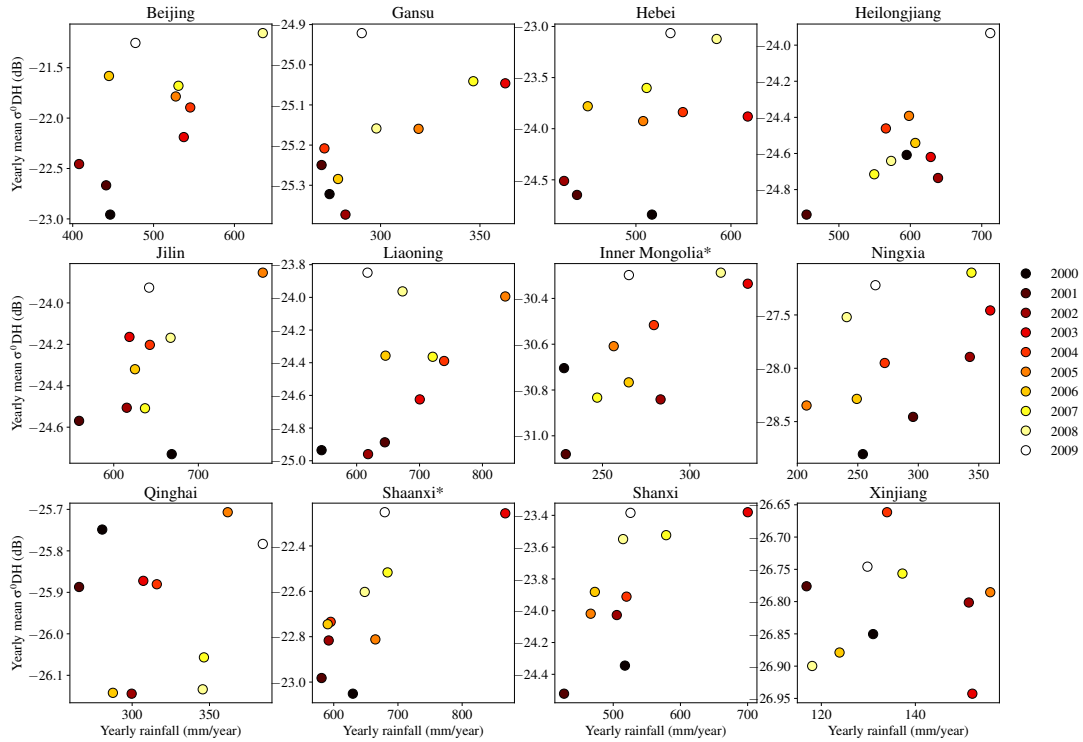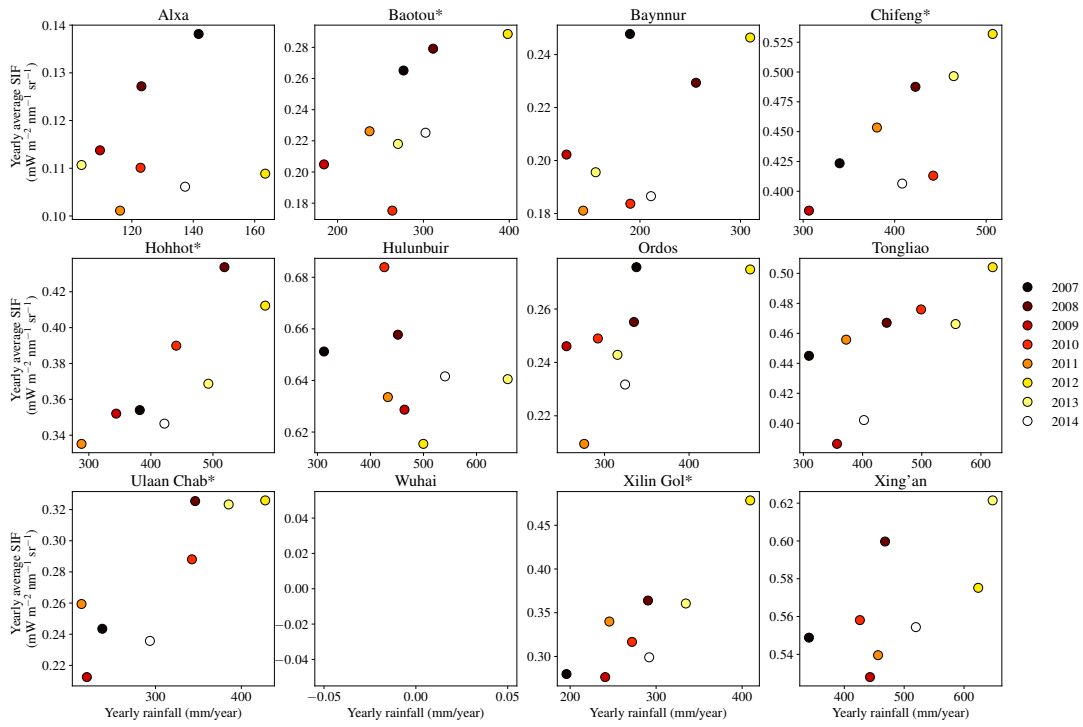

Figure S13: *Yearly average σ_{DH}^{0} signal as a function of yearly rainfall for each province in the TNSP. '*' indicates a significant correlation.*

Figure S14: *Yearly average SIF signal as a function of yearly rainfall for each sub-province in Inner Mongolia. '*'
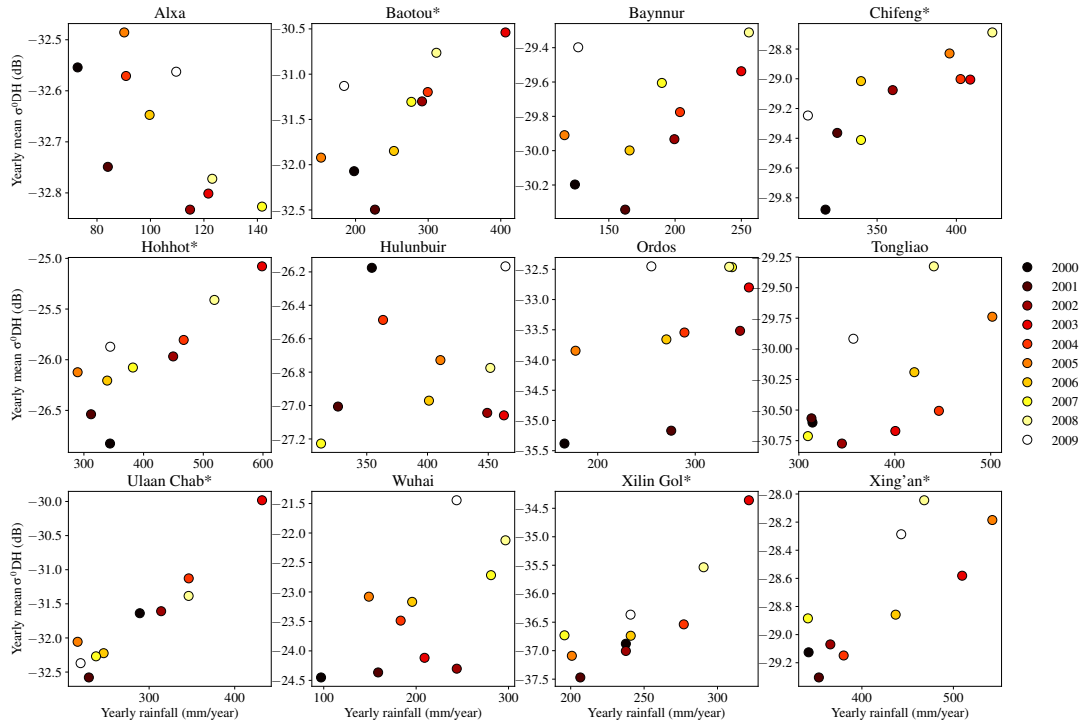indicates a significant correlation.*

Figure S15: *Yearly average σ_{DH}^{0} signal as a function of yearly rainfall for each sub-province in Inner Mongolia. '*'
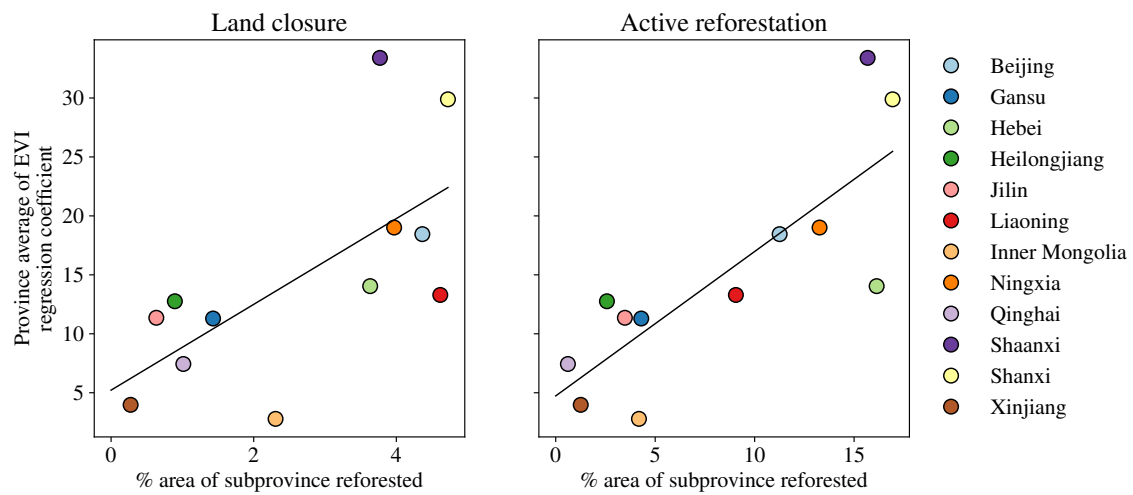indicates a significant correlation.*

Figure S16: *Average slopes of EVI for each province as a function of the percentage of the province reforested by 1) land closure (left), 2) active reforestation (right). Lines show the best linear regression in each case. Land closure: $R^2 = 0.45$. Active reforestation: $R^2 = 0.66$, all with $p < 0.001$.*